

Experimental studies on New Zealand hot spring sinters: rates of growth and textural development¹

B.W. Mountain, L.G. Benning, and J.A. Boerema

Abstract: To study the rate of growth of sinters in New Zealand hot springs, field experiments were conducted in seven geothermal areas. At Wairakei, fan-shaped subaqueous deposits of amorphous silica grow rapidly ($350 \text{ kg a}^{-1} \text{ m}^{-2}$ of drain wall) and are composed of silicified filaments with subordinate bacillus and spirillum-shaped organisms. Characterization of bacteria revealed isolates sharing > 97% 16S rRNA gene sequence homologies affiliated with *Thermus*, *Meiothermus*, *Bacillus*, *Tepidomonas*, *Thermomonas*, *Porphyrobacter*, *Thermonema*, and *Hydrogenophilus* spp., as well as previously uncultured bacteria. At Rotokawa, microstromatolites have a slow growth rate ($0.004 \text{ mm day}^{-1}$) that is attributed to low pH, capillary rise, and evaporation. At Champagne Pool, sinter growth ($0.023 \text{ mm day}^{-1}$) is dominated by wave action building alternating microbe-rich and microbe-poor layers. Silica sinter was not observed at Waikite, where slides developed a layer of calcite ($0.026 \text{ mm day}^{-1}$). Sinter growth at Ngatamariki ($0.016 \text{ mm day}^{-1}$) forms by capillary rise, evaporation, and diffusion and at Tokaanu, subaqueous growth is slow ($0.002 \text{ mm day}^{-1}$) and contains silicified microbes. Textures at Orakei Korako indicate similar mechanisms to Ngatamariki, except that growth is more rapid ($0.023 \text{ mm day}^{-1}$) due to a splash contribution. Silica and calcite saturation indices adequately explain the growth of the sinters and calcite, indicating that microbes are not inducing precipitation where it should not occur. The rate of precipitation is correlated with silica supersaturation, but pH effects can alter this relationship. The degree of preservation of microbial material is explained by the effect of Ostwald ripening on silica spherules. Subaqueous growth allows coarsening of spherules and poor preservation of smaller microbes while subaerial nucleation is rapid, Ostwald ripening is inactive, and better preservation can be expected.

Résumé : Afin d'étudier le taux de croissance des tufs dans les sources chaudes de la Nouvelle-Zélande, des expériences de terrain ont été effectuées dans sept endroits de sources géothermales. À Wairakei, les dépôts subaquatiques de silice amorphe en forme d'éventail ont crû rapidement ($350 \text{ kg an}^{-1} \text{ m}^{-2}$ de paroi de drain) et ils sont composés de filaments silicifiés avec des bactéries et des organismes spiralés subordonnés. La caractérisation des bactéries a révélé des isolats partageant >97 % des homologies de la séquence génétique 16S ARNr affiliées à *Thermus*, *Meiothermus*, *Bacillus*, *Tepidomonas*, *Thermomonas*, *Porphyrobacter*, *Thermonema* et *Hydrogenophilus* spp. ainsi que des bactéries non cultivées auparavant. À Rotokawa, des microstromatolites ont un faible taux de croissance ($0,004 \text{ mm j}^{-1}$) qui est attribué au faible pH, à la remontée capillaire et à l'évaporation. À Champagne Pool, la croissance du tuf ($0,023 \text{ mm j}^{-1}$) est dominée par l'action des vagues édifiant en alternance des couches riches et pauvres en microbes. On n'a pas observé de tuf siliceux à Waikite, où des glissements ont permis le développement d'une couche de calcite ($0,026 \text{ mm j}^{-1}$). À Ngatamariki, le tuf croît à un taux de $0,016 \text{ mm j}^{-1}$ par remontée capillaire, évaporation et diffusion et à Tokaanu, le taux de croissance subaquatique est lent ($0,002 \text{ mm j}^{-1}$); ce tuf contient des microbes silicifiés. Les textures à Orakei Korako démontrent des mécanismes similaires à ceux de Ngatamariki à l'exception d'un taux de croissance supérieur ($0,023 \text{ mm j}^{-1}$) grâce à l'éclaboussement qui y contribue. Les indices de saturation en silice et en calcite expliquent adéquatement la croissance du tuf et de la calcite, indiquant que les microbes ne causent la précipitation que là où elle devrait avoir lieu. Le taux de précipitation est corrélé à la sursaturation en silice mais les effets du pH peuvent modifier cette relation. Le degré de préservation du matériel microbien est expliqué par le mécanisme de mûrissement d'Ostwald sur les sphérules de silice. La croissance subaquatique permet de plus grosses sphérules et une piètre conservation des microbes plus petits alors que la nucléation sub-aérienne est rapide, le mécanisme de mûrissement d'Ostwald est inactif et l'on peut s'attendre à une préservation supérieure.

[Traduit par la Rédaction]

Received 5 February 2003. Accepted June 17 2003. Published on the NRC Research Press Web site at <http://cjcs.nrc.ca> on 26 November 2003.

Paper handled by Associate Editor B. Chatterton.

B.W. Mountain.² Institute of Geological and Nuclear Sciences, Wairakei Research Centre, Private Bag 2000, Taupo, New Zealand.

L.G. Benning. School of Earth Sciences, University of Leeds, Leeds, United Kingdom.

J.A. Boerema. The Horticulture and Food Research Institute of New Zealand, Hamilton, New Zealand.

¹This article is one of a selection of papers published in this Special Issue on *Sedimentology of hot spring systems*.

²Corresponding author (e-mail: b.mountain@gns.cri.nz).

Introduction

New Zealand geothermal areas represent the surface expression of high enthalpy geothermal activity at depth. Within each geothermal field, the distribution of steaming ground, geysers, mud pots, and thermal springs is controlled by local structural, lithologic, topographic, and hydrologic parameters. Deposits of opaline silica sinter, developed as a result of cooling and evaporation of discharging fluids, are found around most of the thermal springs. Within these sinters, extensive evidence is found of thermophilic microorganisms that have contributed, in combination with abiotic factors, to the growth of a variety of textural types. The incorporation of microorganisms in sinter deposits and their contribution to textural development is not a new discovery (Weed 1889). More recently, the recognition that some of these textures resemble ancient stromatolites has led to renewed interest in microbial silicification (Walter et al. 1972). Concurrently, microbiological studies began to elucidate details on the bacterial communities present in New Zealand hot springs (Brock and Brock 1971). Textural studies of New Zealand sinters have further demonstrated the importance of microorganisms to the textural development of sinter deposits (Campbell et al. 2002; Jones et al. 1997, 1998, 1999a, 1999b, 2000, 2001a; Renaut et al. 1996).

Despite the recognition that thermophilic organisms are important substrates for silica precipitation, the question as to whether microorganisms play an active or passive role in silica precipitation is still unresolved. Walter et al. (1972) concluded that silicification of microbial material was a passive process and due simply to changes in physicochemical conditions inducing precipitation. Later studies have shown that microbial material, such as cell walls and extracellular polysaccharides, can be a preferred site of silica nucleation (Ferris et al. 1986; Konhauser and Ferris 1996; Phoenix et al. 1999, 2000; Konhauser et al. 2001). The question as to whether silicification is entirely passive or microbially promoted remains unanswered and is currently a subject of continued study (Benning et al. 2002; Yee et al. 2003).

The majority of studies on silica sinters have focussed on textural features and biofacies in natural deposits. The objectives of such studies were to determine the textural types present, the role microorganisms played in their formation, and the community of organisms responsible based on "fossil" evidence. This study also addresses these questions but the approach has been extended to include experimental studies in which "artificial" sinters were precipitated on glass substrates. This allows observation of the early development of the deposits, their relationship with living and dead organisms, changes in biofacies, and measurement of sinter growth rates. Field-based studies of silica sinter growth using artificial substrates are few (e.g., Inagaki et al. 1997; Konhauser et al. 2001; McKenzie et al. 2001), largely due to slow rates of sinter growth and the need to make regular visits to sample sites that are geographically inconvenient. Glass slides were collected at periodic intervals allowing measurement of growth rates and observation of textural changes. Imaging techniques applied to the samples included scanning electron microscopy (SEM) and transmission electron microscopy (TEM). This is an on-going study with many slides awaiting collection. Phylo-

Fig. 1. Location of study areas in the Taupo Volcanic Zone (TVZ). Dashed line is the approximate boundary of the TVZ. Small filled circles are other geothermal areas not mentioned in this study.

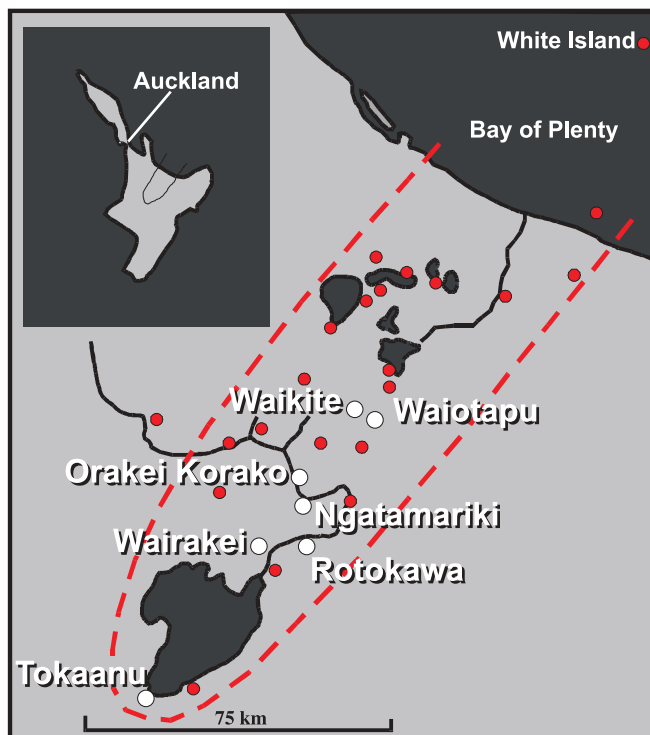


Table 1. Location, pH, and temperature of experiments.

System	Location	pH	T ($^{\circ}\text{C}$) ^a
Wairakei	Main wastewater drain	8.5	49–62
Rotokawa	Spring RK2, sinter flat	3.0	60–85
Waiotapu	Champagne Pool	5.5	71–75
Waikite	Artificial Terrace	7.6	50–100
Ngatamariki	Pavlova Spring	7.2	75–83
Orakei Korako	Tim & Terry geyser	8.2	76–90
Tokaanu	Healy bore 2	7.5	56–62

^aTemperature ranges are those encountered in the immediate vicinity of the experiments.

genetic studies are also underway and preliminary results are reported in this contribution.

Seven geothermal areas were chosen for this study, including Wairakei Power Station main wastewater drain, Champagne Pool at Waiotapu, Rotokawa Sinter Flat, Waikite Artificial Terrace, Ngatamariki, Tokaanu, and Orakei Korako (Fig. 1; Table 1). These areas were chosen for their diversity of chemistries, physical characteristics, location, and accessibility. They are all located within the Taupo Volcanic Zone (TVZ), a subduction-related, rifting arc extending from Mt. Ruapehu in the south to White Island in the north (Wilson et al. 1995). The TVZ is characterized by voluminous rhyolitic deposits with lesser amounts of andesite, dacite, and basalt.

This contribution reports results from our field experiments encompassing the period from March 2001 to December 2002. Silica sinters formed both subaqueously and subaerially on glass slides, and the presence of microbes was confirmed

by microscopic techniques or inferred from sinter textures at all localities. The presence of sinter and their textural development are explained by a combination of chemical principles and differing hydrodynamic regimes at each locality.

Methods

In March and April 2001, glass substrates (25 × 75 mm microscope slides) were placed in thermal waters at each sample site. At Wairakei, the slides were fastened to plastic racks that were suspended in the wastewater drain. At Rotokawa, Ngatamariki, Waikite, and Tokaanu, similar racks were used and were placed in the thermal waters in a horizontal orientation. At Champagne Pool and Orakei Korako, the thermal pools are frequented by tourists. This required placement of slides without racks. At each locality, temperature and pH (± 0.05 units) were measured using a pH meter with attached temperature probe and combination electrode calibrated using two pH buffers heated to near in situ conditions. Filtered ($< 0.2 \mu\text{m}$) water samples were collected for anions (unacidified), cations (acidified to 0.5% HNO_3), and in rubber-sealed bottles for HCO_3^- , H_2S , and NH_3 . Anions (F^- , Cl^- , Br^- , SO_4^{2-} , PO_4^{3-} , NO_3^-) were determined on a Dionex 300 ion chromatograph. Sodium and potassium were measured by atomic absorption spectroscopy on a Perkin-Elmer AAnalyst 800 spectrophotometer using standard methods. Other cations (Li, Ca, Mg, B, SiO_2 , Al, Fe, As, Mn) were measured by inductively coupled plasma optical emission spectroscopy using a Thermo Jarell Ash IRIS spectrophotometer. NH_3 concentrations were measured using an ORION pH/ISE meter equipped with a gas sensing electrode, and concentrations of HCO_3^- and H_2S were determined by manual titration according to the methods of Giggenbach and Goguel (1989).

Solid samples were collected at each location periodically from April. Samples for SEM and TEM analysis were collected into 2.5% glutaraldehyde, and those for petrographic examination were taken dry. All samples were collected and stored in either gamma-sterilized 50 mL falcon tubes or 1.5 mL Eppendorf tubes and kept refrigerated at 4 °C until use. Samples for SEM and TEM analyses were washed twice with phosphate buffer (pH = 7.5), followed by a series of dehydration exchange steps in ethanol (25%, 40%, 60%, 80%, 100%). For SEM, in some cases, this was followed by critical point drying in liquid CO_2 at 31.5 °C. SEM analysis was done on a CamScan 4 instrument equipped with an Oxford MicroAnalysis 10/25S energy dispersive spectrometer operating at an acceleration voltage of 20 kV. TEM samples were embedded in Araldite resin after fixation. They were sectioned to ~ 60 nm on a Reichert-Jung Ultracut-E ultramicrotome and mounted on Formvar carbon-coated 200 mesh copper grids. To improve contrast, the TEM samples were stained with either osmium tetroxide or uranyl acetate. TEM analysis was done on a Phillips CM10 instrument.

For phylogenetic studies at Wairakei, thermal water was collected using aseptic techniques and maintained at ambient temperature. Microbiological media was inoculated with sub-samples (0.1–1 mL) of collected water and incubated at temperatures ranging from 30–60 °C. Microbial growth, as indicated by turbidity in liquid media, or colonies on agar plates, was sub-cultured on solid media. Morphologically

distinct colonies were selected (using size, colour, margin, elevation, and consistency as parameters) and sub-cultured on solid media until deemed to be pure, i.e., of a single morphotype. Pure cultures were subsequently stored in glycerol at $-80 \text{ }^\circ\text{C}$.

Pure cultures were revived from storage by enrichment in liquid media and incubation at their respective isolation temperature until significant turbidity was observed. One millilitre of the resulting suspension was used for isolation of total genomic DNA (Wizard Genomic DNA purification kit, Promega), according to the manufacturer's recommendations. 16S rDNA was amplified by using the bacteria-specific primer pair 27F and 1492R (Lane 1991) and PCR (polymerase chain reaction) conditions described by Broda et al. (1999). The PCR products were purified using the Wizard PCR Prep purification system (Promega) and sequenced directly in an ABI 377 automated sequencer (Perkin Elmer, Applied Biosystems). The phylogenetic affiliation of each partial 16S rRNA gene sequence (~600 nucleotides) was determined using the Basic Local Alignment Search Tool (BLAST) network service (Altschul et al. 1990).

Site details and results

Wairakei Power Station wastewater drain

The main drain at the Wairakei Power Station disposes waste geothermal fluid from the Wairakei borefield. It consists of a concrete channel 3 m wide and 1.2 m deep and is split into two sub-drains by a concrete divider (Fig. 2A). In March 2001, the temperature in the right sub-drain was consistently 62 °C from surface to bottom, while in the left sub-drain, the temperature was 62 °C at the surface and 49 °C at the bottom (Fig. 2A). The temperature gradient is caused by the breaching of the concrete divider further upstream by the high-temperature water in the right sub-drain. The flow rate in the drains is ~ 0.13 m s⁻¹, which represents a fluid flux of about 100 kg s⁻¹ in each sub-drain.

The chemical composition of the wastewater is consistent throughout the main drain. The water has flashed to atmospheric pressure and has lost most of its dissolved gases (mostly CO_2), resulting in a basic pH (Table 2). Sinter deposits in the wastewater drains consist of large (up to 0.5 m) three-dimensional, fan-shaped accumulations attached to the concrete walls of the drain (Fig. 2B). The tips of these structures point downstream, and their size and frequency is presumably controlled by the hydrodynamics of fluid flow. The fans are normally white to pink, but after a heavy rainfall, they become dark brown due to trapping of suspended material washed into the drain. They are composed of amorphous silica (opal-A) and show no sharp peaks under X-ray diffraction analysis (Smith et al. 2001). Underwater examination of the fans (using a glass-bottom container) showed that the tips are extremely fine and are moving in the current (Fig. 2C).

Experimental studies were initiated in March 2001, when racks containing glass microscope slides were suspended from a concrete bridge crossing the drain. After 34 days, the racks were completely covered with a thick coating of fibrous silica (Fig. 2D). It was not possible to collect glass slides without losing considerable precipitate, making it impossible to estimate growth rate. In a second experiment, samples were collected

Fig. 2. Silica sinter deposits in Wairakei Power Station wastewater drain. (A) Schematic isometric diagram of concrete wastewater drain. Gray arrow points in the flow direction. Light gray deposits consist of predominantly silicified filamentous material. Darker gray deposits consist of silicified green microorganisms, assumed to be cyanobacteria. (B) Photograph of wastewater drain showing extensive siliceous fan-shaped deposits. Tips of fans point downstream. (C) Underwater close-up photograph of tip of siliceous fan. Terminal filaments are supple and move in the current. Field of view = 5 cm. (D) Plastic rack containing slides one month after placement in the wastewater drain. The rack is completely encased in a deposit of fibrous silica sinter. (E) SEM photomicrograph of glass slide after 23 h in the wastewater drain. The dark gray areas are uncolonized glass. The slide is covered with fine filamentous organisms with subordinate bacilli. Scale bar = 6 μm . (F) SEM photomicrograph of glass slide after 47 h in wastewater drain. Fine filaments seen in (E) have now been extensively mineralized with silica and have thickened considerably. Also present are silicified bacilli and spirillum-shaped organisms. Scale bar = 6 μm . Inset diagram shows close-up of an encrusted bacillus surrounded by silica spherules of uniform size. Scale bar = 600 nm. (G) SEM photomicrograph of glass slide after 17 h in wastewater drain. Only a few filaments are present. Scale bar = 17.1 μm . (H) SEM photomicrograph of glass slide after 29 h in wastewater drain. The slide is completely covered with fine filamentous organisms. Scale bar = 17.1 μm .

over shorter intervals for a period of 13 days. Samples were air-dried, but not dehydrated, as this causes the fragile silica to disintegrate. Fig. 3 shows the weight of silica mineralization (with contained pore water) precipitated on the glass slides over time. For the first 28 h, no statistically meaningful weights were measured when compared with an average blank slide. After 100 h, a significant amount of precipitate had formed and this continued to increase over the next 200 h. Using these data, an estimate of the average growth rate of silica mineralization of $350 \text{ kg a}^{-1} \text{ m}^{-2}$ of drain wall was made. This rate includes pore water, and without knowledge of the porosity and density of the amorphous silica, it cannot be further refined. The rate is consistent with what is observed over longer periods, as every six months or so, it is necessary to clean the silica deposits out of the drains to prevent blockage.

SEM examination of silica precipitates was done on a third set of samples collected periodically from the right sub-drain. After 1.5 h, small spots ($\sim 50 \text{ nm}$) of amorphous silica were distributed evenly over the slide. After 5 h, the substrate showed the presence of small fragments ($<10 \mu\text{m}$ in diameter) of fibrous silica that represent pieces of silica precipitate that had broken off upstream and had become attached to the slide. The mechanisms of this attachment is unknown but is possibly related to biota. After 23 h, the slide was covered with a coating of fine filaments about 100 nm in width and of unknown length (Fig. 2E). The filaments are of uniform width, are non-branching and lie in preferred orientations. SEM-EDS (energy dispersive spectroscopy) analysis of the filaments shows only Si, thus the filaments are assumed to be composed of opal-A. Also present were bacillus-shaped organisms 0.6 μm in width and up to 3 μm in length. Increased silicification of the filaments was found in the sample collected at 47 h. Along with filaments similar to those observed at 23 h, the slide was now covered with interlocking tubes 0.5 μm in diameter that represent thickened silicified filaments deposited earlier (Fig. 2F). The bacillus-shaped organisms were thicker with a continuous coating of silica along with numerous spherules of abiotic silica (defined as silica spherules unattached directly to biological material). Also present are the silicified spirillum-shaped bacteria.

The macroscopic and microscopic textures of silica mineralization at Wairakei indicate that the fine filaments compose the bulk substrate for silica growth. These filaments could be microorganisms or silicified exudates, such as polypeptide or polysaccharide chains, excreted by microbes further upstream.

To investigate this, a fourth experiment was undertaken in which glass slides were collected over a 29-h period at 2–4-h intervals. This allowed closer examination of the initiation and growth of the mineralization. After 17 h, the slides showed only a few isolated filaments (Fig. 2G). Over the next 12 h, the number of filaments increased rapidly, and on the final slide (at 29 h), the whole surface was covered with extensive growth (Fig. 2H). These results indicate that the rate of growth is more exponential than linear with time consistent with the growth of microorganisms (Prescott et al. 2002). Trapping and silicification of exudates would be expected to be linear with time, and it is concluded that the silica filaments are the result of silicification of filamentous organisms. The identity of these organisms is the subject of further study.

Significant microbial diversity was revealed in the samples collected from the Wairakei drains using culture-based methods. Twenty-seven phylogenetically distinct bacterial sequence types were determined by partial, or near complete, 16S rRNA gene sequence analysis. Isolates sharing $> 97\%$ 16S rRNA gene sequence homologies with sequences in GenBank were affiliated with *Thermus*, *Meiothermus*, *Bacillus*, *Tepidomonas*, *Thermomonas*, *Porphyrobacter*, *Thermonema*, *Hydrogenophilus* spp., and previously uncultured bacteria. All isolates obtained in the cultivation studies yielded 16S rDNA gene products with primers specific for the phylogenetic domain *Bacteria*, however, the presence of *Archaea* in the Wairakei thermal waters is indicated by the identification of archaeal lipids extracted from the silica mineralization and analyzed by gas chromatographic mass spectrometry (Pancost et al. 2002).

Rotokawa

The Rotokawa geothermal field lies 8 km to the northeast of Wairakei (Fig. 1). The highest density of thermal features is located immediately north of Lake Rotokawa with the largest being an accumulation of hot springs (up to $90 \text{ }^\circ\text{C}$) of $\sim 0.07 \text{ km}^2$ in area forming a small thermal lake. This lake is surrounded by a sinter flat formed of finely laminated silica interbedded with unconsolidated mud deposits. The majority of the hot springs at Rotokawa can be classed as the acid sulfate type and are derived by mixing of deep aquifer water with steam-heated waters rich in H_2S . This subsequently undergoes oxidation near surface creating high sulfate concentrations and high acidity (Krupp and Seward 1987, 1990). Jones et al. (2000) studied the microstromatolites that occur along the southeast margin of the hot-springs lake and

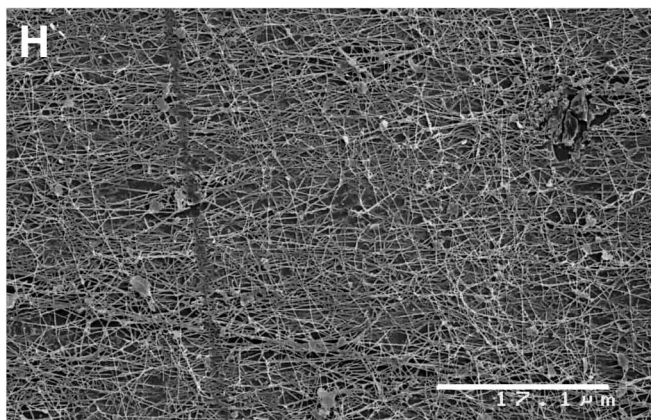
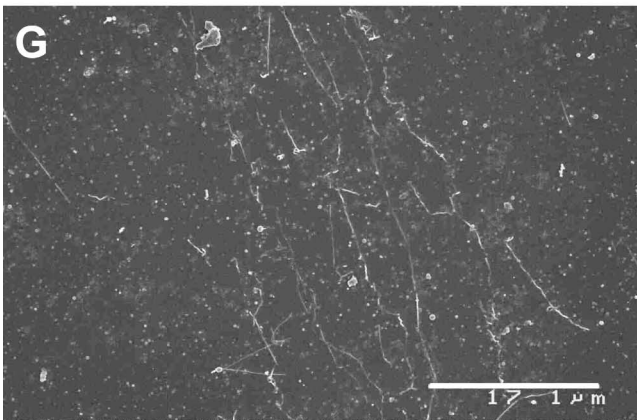
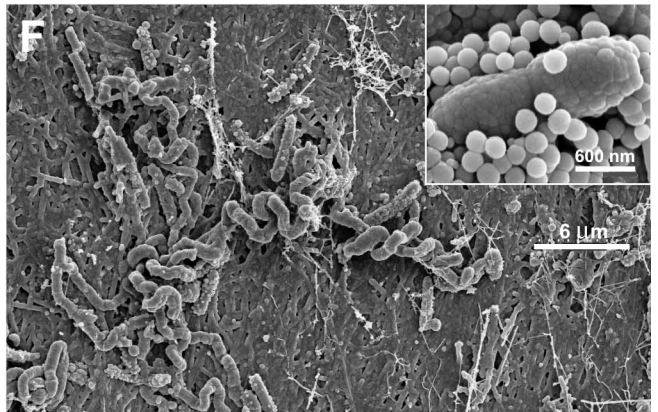
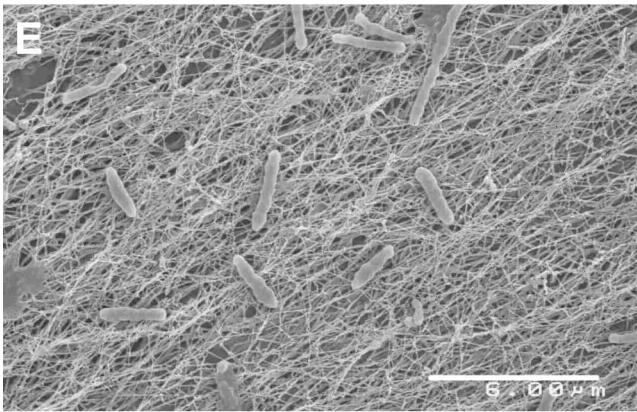
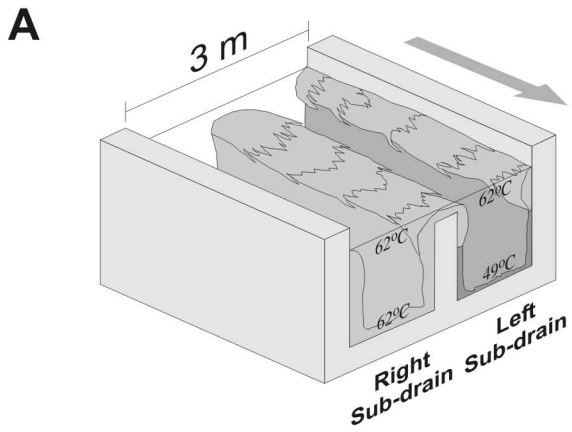


Table 2. Chemical composition and temperature at sampling of waters from New Zealand geothermal localities referred to in this study.^a

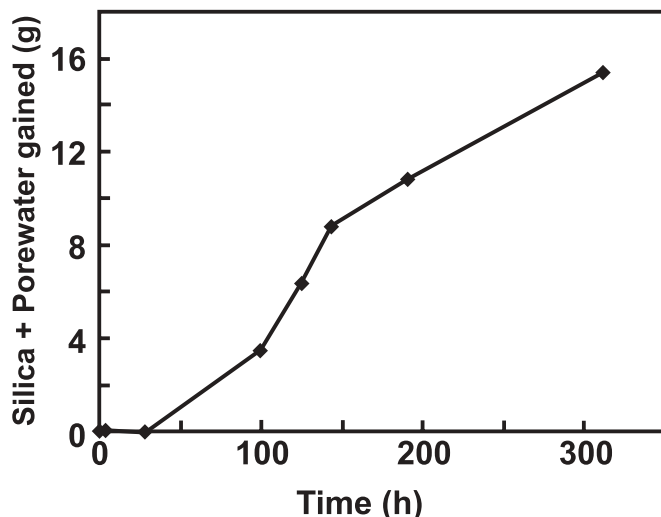
Location	Date	<i>T</i> (°C)	pH ^b	Li	Na	K	Mg	Ca	B	Al	Fe	Mn	SiO ₂
Wairakei Main drain	27/03/01	62	8.23	10.7	1127	155	<0.01	19.6	25	0.57	0.05	<0.01	559
Rotokawa Pool RK2	30/03/01	85	3.01	6.8	824	88	3.6	31	41	4.9	0.33	0.58	333
Champagne Pool, north side	4/04/01	75	5.46	8.7	1134	161	0.04	33	24	0.19	0.04	0.08	430
Waikite Artificial Terrace	6/04/01	99	7.60	2.6	214	6.6	0.18	7.7	1.5	<0.1	0.03	0.07	149
Ngatamariki, Pavlova Spring	9/04/01	83	7.22	3.6	533	29	0.44	7.3	8.7	<0.1	0.02	0.06	234
Orakei Korako geyser	4/04/01	99	8.17 ^c	3.9	315	52	0.02	1.8	3.4	<0.1	<0.02	0.01	319
Tokaanu, Healy bore 2	6/04/01	93	7.54	16.6	1274	100	0.7	55	65	<0.1	0.08	0.10	290

Table 2 (concluded).

Location	As	Cl	HCO ₃	H ₂ S	SO ₄	NO ₃	PO ₄	F	Br	NH ₃
Wairakei Main drain	4.0	1958	9.3	<0.2	45	<0.02	<0.04	8.5	3.8	0.2
Rotokawa Pool RK2	0.64	1198	<1	16	622	<0.02	<0.04	3.2	2.2	n.m. ^d
Champagne Pool, north side	4.7	1926	153	7	165	<0.02	<0.04	5.5	4.3	36
Waikite Artificial Terrace	0.3	146	327	0.5	90	<0.02	<0.04	2.6	<0.03	0.6
Ngatamariki, Pavlova Spring	<0.1	567	478	0.7	45	<0.02	<0.04	2.4	1.1	n.m. ^d
Orakei Korako geyser	0.55	334	178	0.4	102	<0.02	<0.04	11	0.88	0.21
Tokaanu, Healy bore 2	6.0	2104	25	0.3	90	<0.02	<0.04	1.2	5.1	4.6

^aConcentrations in mg kg⁻¹.^bIn situ pH measured using buffers heated to approximate pool temperature.^cCalculated from room temperature pH.^dn.m., not measured.

Fig. 3. Weight of silica plus entrained porewater deposited on glass slides in Wairakei wastewater drain versus residence time. Over the first 28 h, no meaningful weight could be measured. By 100 h significant mineralization had formed and continued to thicken over the next 200 h. Each data point represents the measured weight of silica plus pore water on one slide (8 in total).



described a continuous band of these structures composed of opaline silica, kaolinite, and sulfur lying parallel to the shoreline. Biota present included bacteria, spores, pollen, diatoms, and fungi. The internal structure of stromatolites consisted of interlayered laminae of opaline silica and darker, clay-rich material.

To estimate the growth rate and study the textural development of the stromatolites, glass slides were placed around the hot springs lake commencing in March 2001. The slides were laid flat so that they were just covered with thermal water. Samples were collected over the next several months. These became covered with either a thin greenish biofilm or with a layer of unconsolidated black mud, formed due to settling of suspended material. No silicification or spicule development was observed. SEM examination of mud samples showed no identifiable microorganisms, but TEM examination revealed a few non-filamentous microbes.

Fluctuating water levels on the sinter flat make short-term experiments difficult, and it was decided to concentrate on one of the ebullient pools in the northeast portion of the sinter flat. Pool RK2 (Fig. 4A) is 1.5 m in diameter and contains turbid water caused by fine suspended clays and native sulfur. The pool water has a typical composition of an acid sulfate pool with high concentrations of SO_4^{2-} and a low pH (Table 2). The water temperature was 85 °C in the centre of the pool in March 2001 and has remained constant since this time. Temperature drops to about 60 °C over several metres as the water flows out in a thin sheet < 1 cm in depth. This shallow depth prevents any significant wave action. The pool and its outflow are at a slightly higher elevation than the adjacent hot lake, thus it is not affected by fluctuating water levels. The fine solids carried in the outflow have built up a layer of mud 3–4 cm thick that lies upon a hard sinter layer. The mud is laminated with gray and green layers containing amorphous arsenic and antimony sulfides.

Isolated microstromatolites populate the outflow of the

pool (Figs. 4A–4D). They are circular to oval in shape with their dimensions determined by the size of the substrate. Most appear to have grown contemporaneously, as the pumice and sinter fragments that core them lie on the same hard sinter layer below the mud. As the mud thickened, they grew upwards and outwards creating coral-shaped structures (Fig. 4C). The microstromatolites are composed of hundreds of laminations that are either (1) light in colour, indicating that they are silica-rich; (2) dark in colour, indicating a high content of clay minerals and sulfur; or (3) orange to yellow, suggesting the presence of high concentrations of As and Sb (Figs. 4C, 4D). Microstromatolites do not display any obvious porosity and are quite hard. The tips of the spicules on each stromatolite protrude above the water and reach a maximum height of ~ 1 cm above the air–water interface (Fig. 4A). Large cavities between the microstromatolite columns have trapped mud deposits, sinter layers and ash from local volcanic activity. Some microstromatolites show evidence of a smooth in-filling covering cavities and the spicular growth in their centres (Fig. 4D).

To estimate the microstromatolite growth rate, a series of glass slides was inserted vertically into the mud at regular distances from the pool in May 2001. After two months, no growth had occurred in the water (Fig. 4E), while at the air–water interface a yellowish layer composed of native sulfur was present. Above the interface, a dark layer of hard silica had grown. This layer has an upward concave shape suggesting capillary action is at least partly responsible for its formation. The silica layer is also covered with numerous irregular protrusions that could be interpreted as the beginnings of spicules. At nine months, the silica layer had become noticeably thicker and fine spicules about 1 mm in length now covered the surface (Fig. 4F). The thickness of silica mineralization was measured in February 2002, and a growth rate of $\sim 0.004 \text{ mm day}^{-1}$ was estimated.

Champagne Pool, Waiotapu

The Waiotapu geothermal system, located 45 km northeast of Wairakei, is the largest area of surface thermal activity in New Zealand (Hedenquist 1986a). The largest chloride spring, the Champagne Pool, is well known for its size and distinctive orange precipitates that contain high concentrations of heavy metals including As, Sb, Au, Ag, Hg, and Tl (Weissberg 1969; Hedenquist 1986a; Hedenquist and Henley 1985; Jones et al. 2001b). The pool is roughly circular in shape with a diameter of ~65 m. Champagne Pool water is of neutral chloride type (Table 2) and is enriched in H_2S , NH_3 , and heavy metals. The water is essentially anaerobic with a dissolved oxygen concentration of 0.03 ppm O_2 (Institute of Geological and Nuclear Sciences (IGNS), New Zealand, unpublished data). Champagne Pool is highly convective and maintains a constant temperature of 75 °C with slightly lower temperatures occurring around the shallow margins.

The morphology of sinter deposits varies around the margins of the pool. Along the northwest, west, and southwest margins, the top of the sinter rim is elevated above the water level, locally as much as 50 cm (Fig. 5A). Between the water's surface and the top of this sinter rim, several ledges of silica mineralization composed of inactive spicular microstromatolites are present (Figs. 5A, 5D). Along the southern margin, earlier sinter rims appear eroded and pass below sand deposits that

Fig. 4. Microstromatolites at Rotokawa. (A) Oblique view of RK2 hot pool. The ebullient pool is in the foreground. Turbid spring water flows outwards in a thin sheet building up unconsolidated mud deposits. Outflow is inhibited by isolated microstromatolites. White arrow points to slides shown in (F). Hot pool is 1.5 m in diameter. (B) Overhead view of pool outflow showing isolated microstromatolites surrounded by mud deposits. The microstromatolites protruded above the water surface by about 1 cm. Pen for scale. (C) The microstromatolite immediately north of the pen in (B) extracted from mud. Microstromatolite growth initiated on the pumice rock at the bottom and is composed of dark clay-rich and light silica-rich laminae. Dashed white line shows approximate level of mud deposits before extraction. Scale is in cm. (D) Cross-section through microstromatolite showing pumice rock base (P), dark and light laminae, entrapped mud and ash deposits (M), and smoother laminae that have covered the central cavity (L). Horizontal dimension of stromatolite is 7 cm. (E) Glass slides placed in the outflow of RK2 pool after two months. The slide is coated with a layer of native sulfur at the air-water interface. Above the water, dark gray nodular silica has grown by capillary rise. Dashed white line emphasizes the upward concave shape of the silica deposits. Note the shallow depth of the water. (F) Glass slides placed in the outflow of RK2 pool after nine months (not the same slides as (E)). The dark gray silica deposits have thickened and spicular growth has developed. Slides are 25 mm along the top dimension.

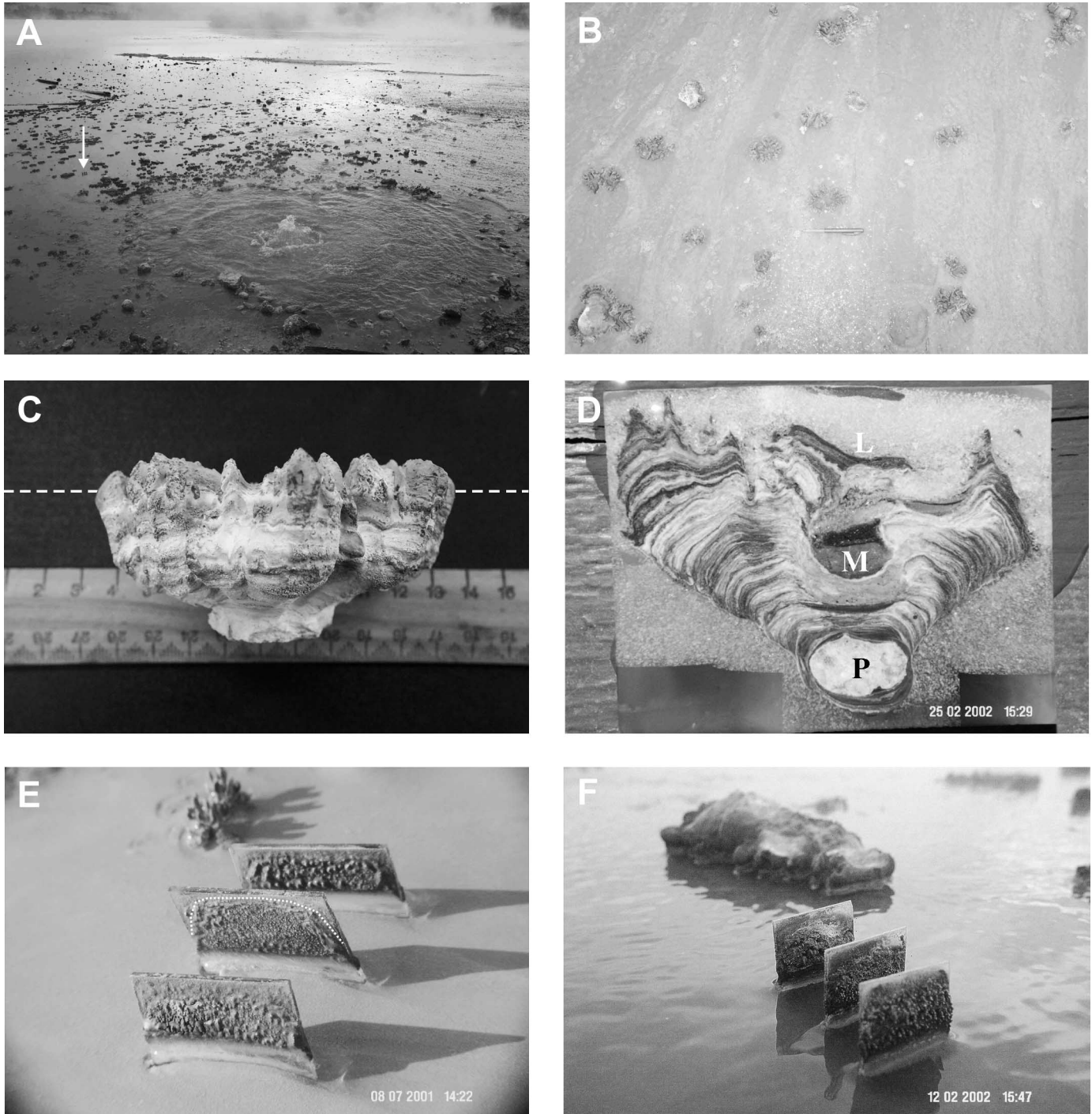
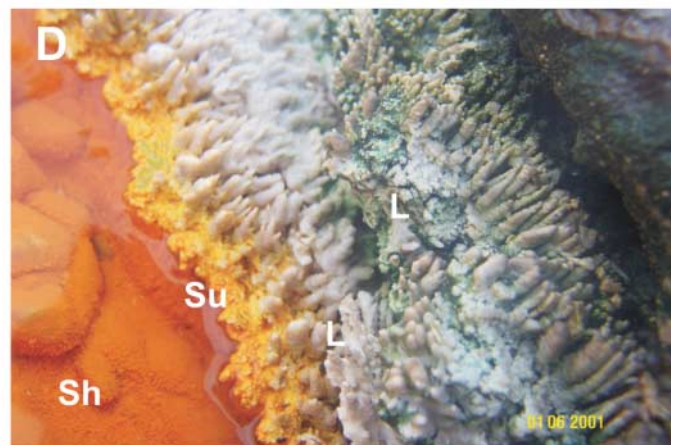
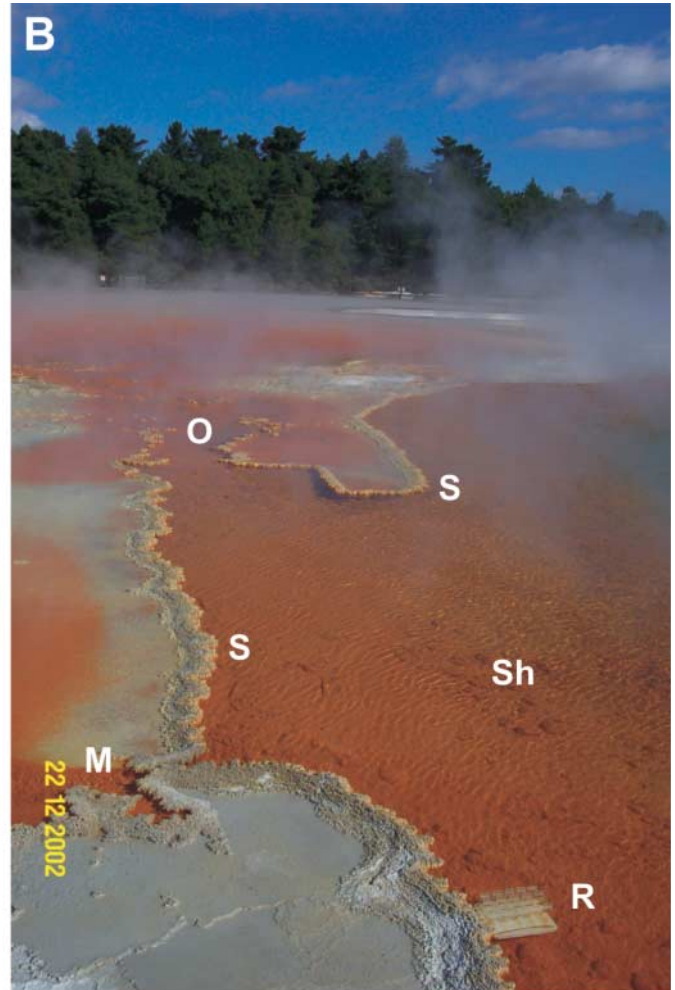
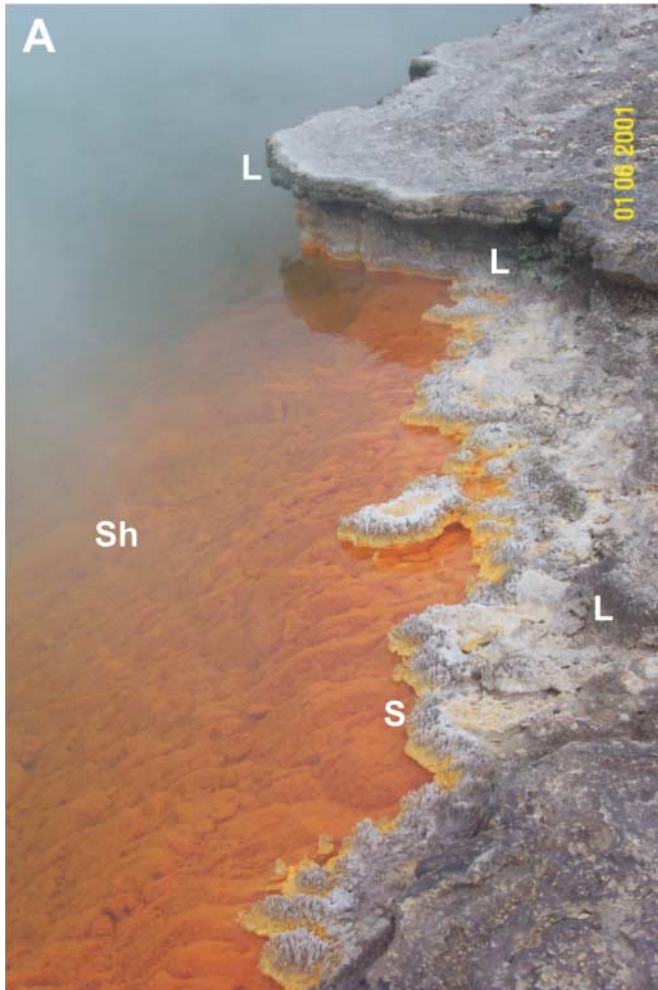


Fig. 5. Macroscopic features of Champagne Pool, Waiotapu. (A) Western pool margin showing raised ledge (~30 cm above water surface) overhanging pool edge (L). At the current water level there is extensive growth of spicular microstromatolites (S). The orange sinter shelf (Sh) is visible below the water surface. (B) Northern pool margin where natural outflow (O) onto the Primose Terrace occurs. The margin of the pool is defined by a narrow sinter rim (S, ~20 cm in width). The subaqueous shelf (Sh) is extensive and remains relatively shallow before dropping off almost vertically. A man made cut in the sinter (M) is lined with microstromatolites. One of the experimental sample racks is in the foreground (R). (C) Close-up view of spicular microstromatolites at the edge of the pool. The subaqueous shelf is to the left (Sh). Field of view = 10 cm. (D) Northern margin of pool showing domal microstromatolites comprising the subaqueous shelf (Sh). At the air-water interface, yellow native sulfur is present (Su), above this are a series of ledges composed of spicular microstromatolites (L). Green growths are cyanobacteria and (or) algae.



have washed down from an adjacent cliff. Along the east margin of the pool, a continuous sinter rim reappears and reaches a maximum elevation of about 10 cm above the water surface. The natural outflow from the pool occurs on the northern margin (Fig. 5B). The outflow is rimmed by a sinter dam about 10–20 cm in width that is composed of spicular microstromatolites that become progressively smaller towards the pool and are currently active (Fig. 5C). The morphology of the sinter dam along the northern margin suggests that it has grown over a period during which the water level has been stable.

In detail, the margins of the pool display a series of bio-mediated silicification features (Fig. 5D). The subaqueous ledge is composed of domal stromatolites containing silicified remnants of microorganisms (Jones et al. 1997). The stromatolites are covered with a coating of unconsolidated orange floc that is filamentous in form and is attached to the stromatolite surface. These filaments are supple and move in the local convection currents or as the result of wave action. Immediately at the air–water interface, a rim of yellow sulfur is present that is continuously washed by pool water. Above this, spicular microstromatolites occur that increase in size with distance from the pool reaching up to 3 cm in height. They are composed of laminated amorphous silica containing preserved microbial remnants. SEM examination of a small microstromatolite spicule shows that their bases are composed of crystalline masses of fine sulfur crystals. A porous mixture of filamentous organisms and sulfur is built upon the sulfur base. The conical portion of the spicule is composed of layers of non-porous silica alternating with porous layers rich in silicified microorganisms (Mountain et al. 2001).

A series of ten slides was placed in the pool in August 2001 that were spaced at 2 cm intervals with their ends protruding ~ 5 mm above the pool surface. After 24 h, a diffuse white coating of silica was visible on the slides. This coating continued to thicken and, by 30 days, small spicules had begun to grow on the tips of the slides. These were 1 mm in height and had a regular spacing of 1 mm along the top of the slides (Fig. 6A). An average growth rate of 0.02 mm day⁻¹ was estimated from these spicules. Below the water surface, a coating of orange filamentous material was attached to the slides and the plastic racks. By November 2001, the spicules had grown larger and were more irregular. During the November sampling trip, it was observed that on this particularly windy day, the amplitude of wave action was about 3 cm, and pool water regularly topped the slides and washed over the sinter rim.

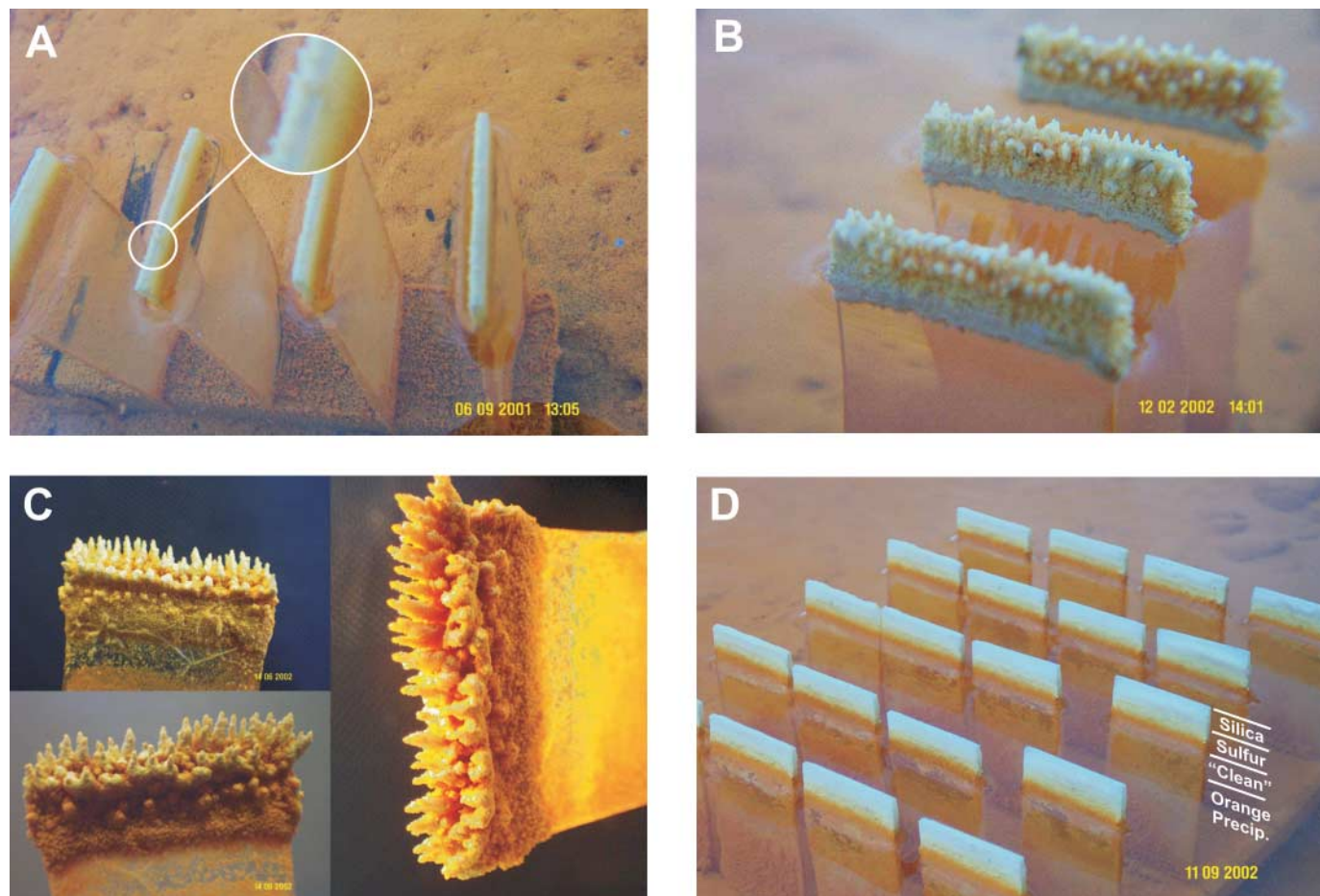
By February 2002, the spicular morphology had developed substantially. Silica precipitates had thickened immediately below the early spicules and secondary spicules had begun to form on this thickened silica (Fig. 6B). Below the water surface, the orange filamentous material was present and near the bottom of the slide, it had become a thick beard-like growth. Between the subaerial silica mineralization and the subaqueous orange filaments, a clean band was observed caused by the washing of the slide by wave action. By June 2002, considerable silica sinter had grown on the slides (Fig. 6C) with individual spicules reaching 7 mm in height. The older spicules on the tops of the slides had a slightly curved axis that bent towards the pool margin. They were

noticeably thicker and merged near their bases. The secondary spicules had continued to grow and a third set was also beginning to develop. The sinter also had considerable amounts of orange floc along the underside of the spicules and in the interstices between them. From the size of the largest spicules an average growth rate of 0.023 mm day⁻¹ was estimated, similar to that estimated in September 2001.

The samples described in the previous paragraphs represent long term experiments and the remaining slides will be collected over the next couple of years to obtain an estimate of lateral growth rates of the sinter margin. To elucidate process occurring early in sinter development, a second series of slides was placed in the pool in July 2001 close to the location of the first set (Fig. 5B).

Samples collected in August and September 2002 have been studied by SEM. Textural development on both slides is similar with precipitates on the later slide being slightly thicker. Figure 6D shows one rack of twenty slides in September 2002, 73 days after emplacement. The slides are covered with a coating of white silica between 5 and 6 mm in vertical dimension that ends at the air–water interface. Below this is a yellow band of native sulfur about 5 mm in width. This is followed by a zone of relatively clean glass also about 5 mm in width. Orange filamentous material covers the remainder of the subaqueous portion of the slides and this coating becomes thicker with depth. In Fig. 7A, the bottom edge of the sulfur zone is shown. At the scale of the photomicrograph, it appears that the slide is clean, however, higher magnification shows the presence of bacillus-shaped microbes (Fig. 7B). They have a high aspect ratio with a uniform width of ~ 0.3 μm and lengths up to 10 μm. The microbes do not appear to be mineralized and have attached themselves to the substrate by fine bipolar fimbriae. Sulfur mineralization occurs as euhedral crystals that lie in preferred orientations indicating that they have grown in place (Fig. 7A). Examination of the sulfur crystals at high magnification shows that they are covered with a biofilm consisting of the microbes surrounded by a complex network of fine filaments (Figs. 7C, 7D) that may represent cannulae with desiccated mucus (Stetter 1998). The microbes have the same morphology as those found attached to the glass slide, and no other morphotypes were observed. Silica laminae or spherules were not present in the sulfur-rich zone. Sulfur mineralization continues up the slide, and there is a noticeable decrease in crystal size upwards (Fig. 7E). A sharp boundary, defined by a prominent textural change, signifies a switch from porous sulfur to laminar silica mineralization. The silica appears smooth at low magnification (Fig. 7E) but at higher magnification can be seen to be composed of thin discontinuous laminae (~5 μm thick) that lie parallel to the slide and enclose abundant pore space (Fig. 7F). This zone of laminated silica is poor in microbes. The laminated silica continues and thickens towards the top of the slide. Before coating for SEM analysis, a sharp knife blade was used to scrape off the silica mineralization from one side of the slide. This exposed a cross section of the silica mineralization on the top of the slide (Fig. 7G). It is composed of non-porous layers of amorphous silica that enclose discontinuous porous layers. The continuity of the layers is evident near the top of the slide but decreases markedly towards the outer surface. The pores are filled with

Fig. 6. Experimental sinter growths on glass slides from Champagne Pool. (A) After 30 days, small spicules (~1 mm) have developed on the top edges of the slides (shown magnified). Plastic holder is covered with growth of filamentous material covered in orange sulfur. (B) After 4 months, spicule morphology is well-established. Rows of secondary spicules had also begun to grow below the top row. (C) Top and side views of glass slide removed in June 2002 (10 months). Spicules had grown to a maximum height of 7 mm. The rows of secondary spicules are well-established and a third row is beginning to grow. Fibrous object in top left view is a bird feather. (D) Rack of glass slides after 2 months. Subaerial portion of slides are covered with white silica. Below this is a band of yellow and orange native sulfur, followed by a band of partially clean glass. A complete coating of orange filamentous material covers the remaining subaqueous portion of the slides. All glass slides are 25 across the top dimension.



filamentous microbial material that may be silicified, although it is not possible to tell with EDS because of the high background concentrations of silica. The outer surface of the mineralization is covered with a dense biofilm of interwoven fine filaments < 200 nm in width and of unknown length (Fig. 7H). The network of filaments drapes over both the nodular amorphous silica and interstitial porous areas. The samples studied by SEM did not show any spicule growth and were even across their tops. To date, microscopic textural information is unavailable on the cause of spicule initiation.

Waikite

The Waikite hot springs are located ~ 10 km northwest of Waiotapu (Fig. 1). Approximately 35 springs emerge over a distance of 1.5 km discharging water between 30 and 99.5 °C (Glover et al. 1992). Most of the springs are surrounded by silica sinter but at least six of the hotter springs also have calcite present. Jones et al. (1996) have reported on the textural characteristics of calcite in the discharge aprons and from

oids in the natural springs. Also located at Waikite is a large artificial terrace, completed in 1972, that is supplied by a single bore.

Glass slides, both restrained in racks and unrestrained, were placed in the artificial terrace in April 2001. The bore supplying the terrace is located at the eastern end and discharges about 5 L s⁻¹ of thermal water with a temperature of 99 °C. Along the terrace, the water temperature decreases from 99 °C at the bore outlet to about 50 °C at the western end. The water has a slightly alkaline pH, is low in SiO₂ and Cl⁻, and contains high HCO₃⁻ (Table 2). This is consistent with meteoric water steam-heated by thermal fluid on the edge of the Waiotapu geothermal system. The terrace has been active for over thirty years and now contains extensive mineralization. The first two thirds of the terrace are covered with a layer of beige calcite mineralization that lines the bottom and rims rocks placed in the flow (Fig. 8A). Where the temperature drops to about 60 °C, calcite mineralization ceases and biomats (up to 5 cm thick) are present (Fig. 8B).

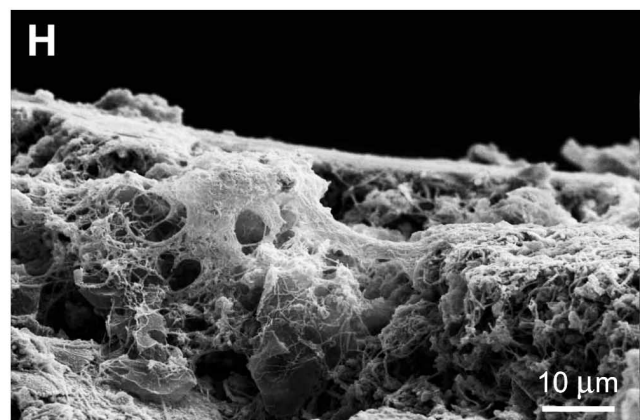
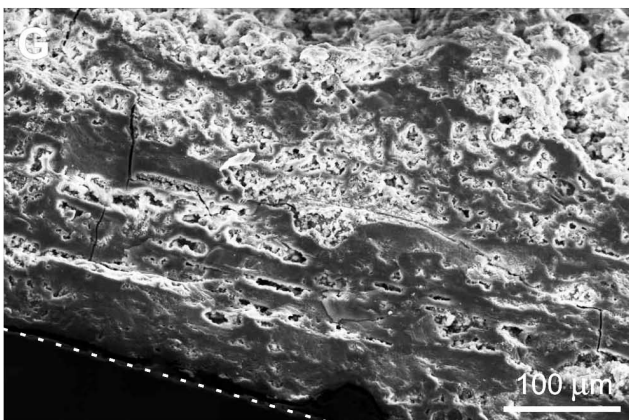
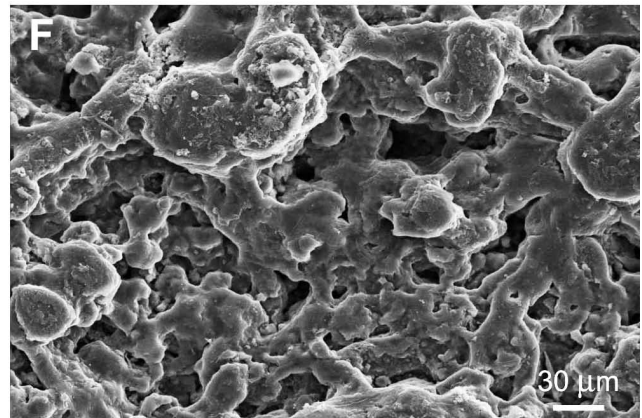
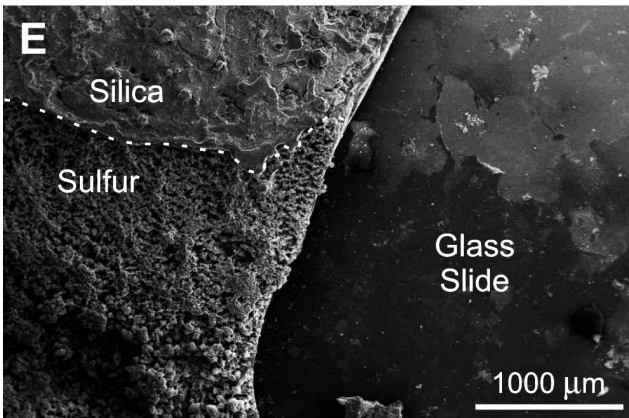
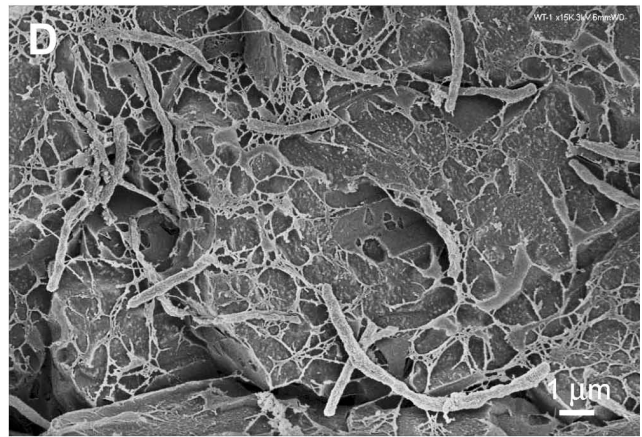
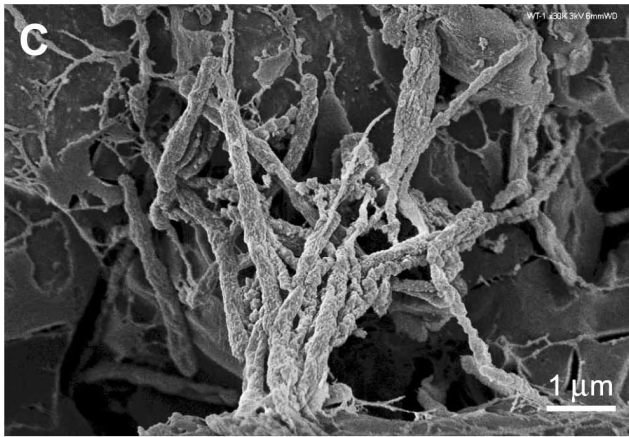
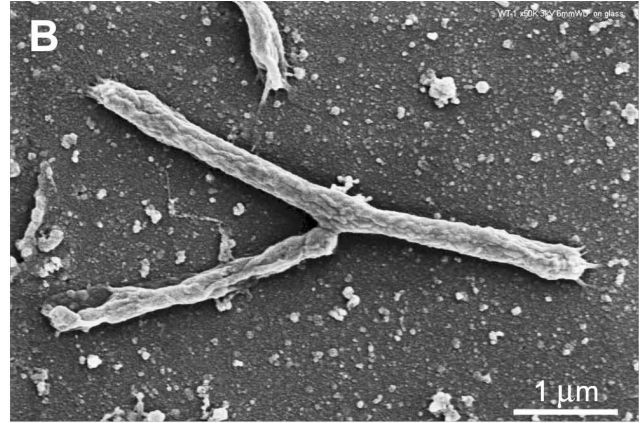
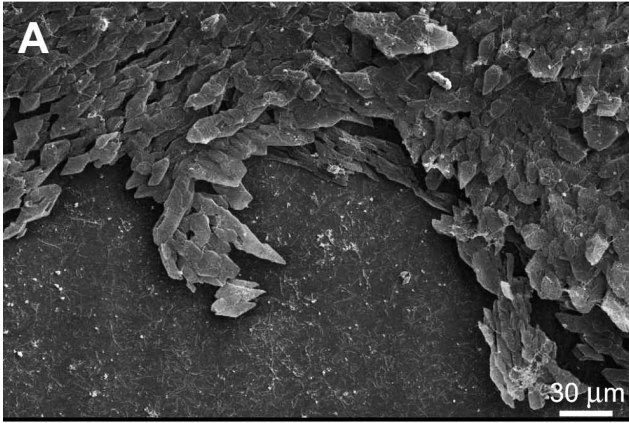
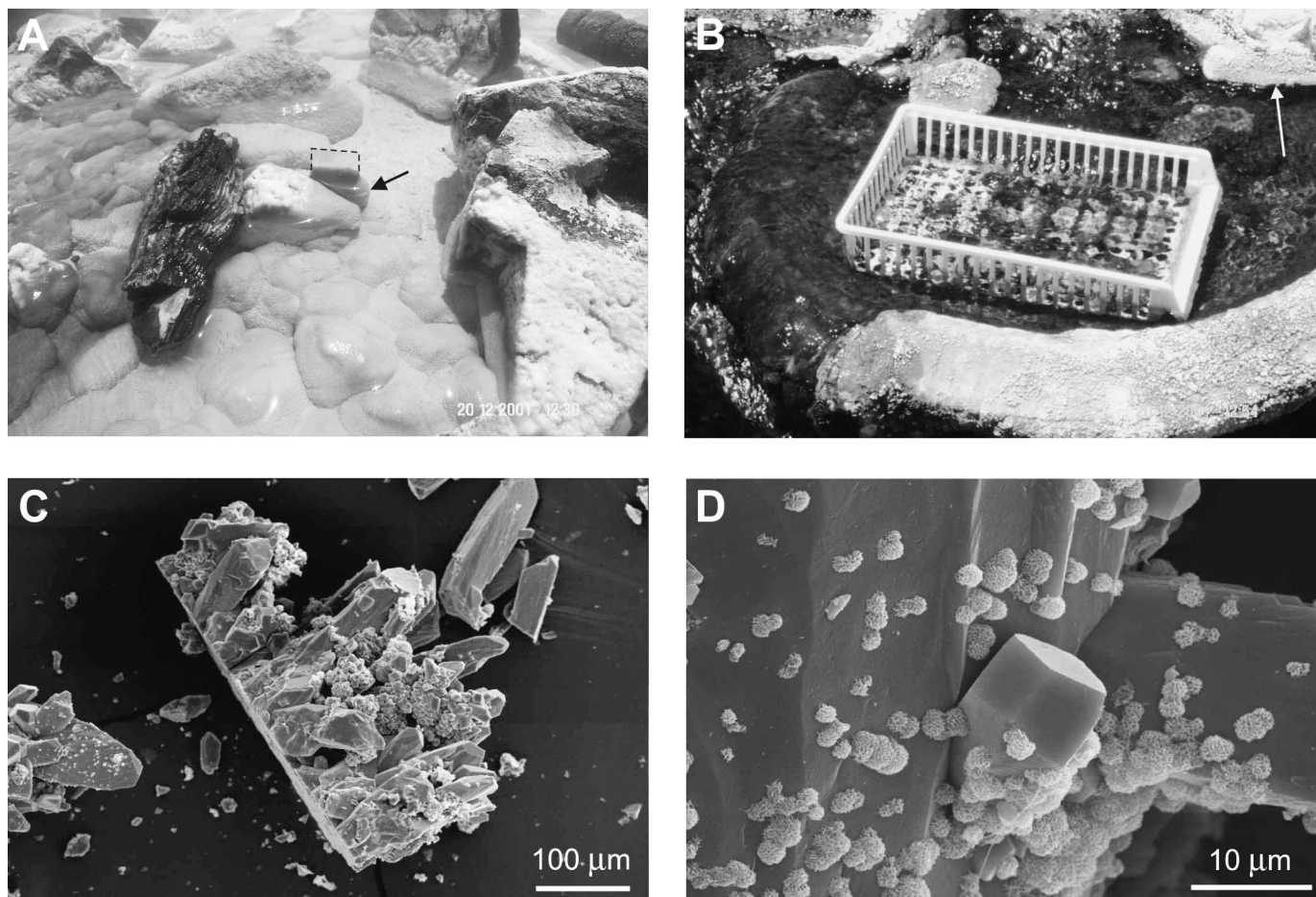


Fig. 7. SEM photomicrographs of experimental growths on glass slides placed in Champagne Pool after 1–2 months. (A) Transition from relatively clean slide to beginning of sulfur zone. Sulfur crystals are euhedral and lie in preferred orientations indicating that they have grown in situ. (B) Bacillus-shaped microorganisms on glass slide just below the sulfur zone. Note the bipolar fimbrae securing the microbes on the slide. (C) An agglomeration of microorganisms attached to sulfur crystals. (D) Bacillus-shaped microorganisms on larger euhedral sulfur crystals surrounded by cannulae or desiccated mucus. (E) Sharp transition from porous sulfur zone to laminar silica zone (dashed line). Dark area to right is the glass slide. Sulfur crystals fine upwards. (F) Closer view of laminar silica zone composed of numerous thin discontinuous layers of silica. This zone is microbe-poor. (G) Silica sinter from top of the slide. Dashed line is the top of the glass slide. Discontinuous porous layers alternate with solid non-porous layers. Pore spaces are filled with abundant microbes. (H) Top of slide after two months. Nodular silica is covered with a fine meshwork of filamentous organisms that drape over pore spaces.

Fig. 8. Calcite and sinter deposits from the artificial terrace at Waikite. (A) Unrestrained slide in area of calcite mineralization on the artificial terrace. Bottom of terrace is covered in a continuous coating for light brown calcite. Dashed line is the outline of the subaerial portion of the glass slide and black arrow points to the subaqueous growth of calcite ($T \approx 75^\circ\text{C}$). Glass slide is 25 mm across top dimension. (B) Plastic tray in plunge pool in the lower temperature ($T \approx 55^\circ\text{C}$) part of the terrace. Dark areas are thick biomats composed of green biota, presumably cyanobacteria. White arrow points to the thin subaerial sinter rim around the plunge pool. Rack is 30 cm long. (C) SEM photomicrograph of calcite crystals. Bimodal grain size is present. (D) SEM photomicrograph of small platy aggregates of unknown mineral phase attached to large calcite crystals.



The biomats form discontinuous layers, globular masses, and conical-shaped bodies (conophytions) within the section of terrace between 55 and 60 °C. The outer surfaces of the biomats are green in colour and their interiors are gray to brown and contain numerous fine laminations. Below 55 °C, the biomats become continuous and cover the entire terrace with a layer about 2 cm in thickness. Silica sinter is present in the lower temperature parts of the terrace and on the edges of plunge pools (Fig 8B), however, there is no evidence of subaqueous silicification of the biomats.

Glass slides have been collected from the artificial terrace on several occasions over a period of 18 months. After one month, the subaqueous portion of glass slides was covered with a thin layer of beige calcite. SEM examination of the calcite shows euhedral to subhedral grains growing approximately perpendicular to the slide (Fig. 8C). The grain size is bimodal with larger grains up to 1 mm forming the bulk of the mineralization, while smaller-sized grains are attached to, and fill interstices between, the larger grains. A second mineral phase was present and consisted of spherical aggregates

up to 2 μm in diameter of a platy mineral (Fig. 8D) that shows a peak for silicon under EDS analysis. The identity of this phase remains uncertain as the water is undersaturated with respect to opal-A (see later in the text). SEM examination showed no evidence of microbes in the calcite or on the surface of the grains nor was any extracellular mucus present. After 8.5 months, the slides were covered on their subaqueous portions by a layer of beige calcite 7 mm thick (Fig. 8A) representing a growth rate of $0.026 \text{ mm day}^{-1}$. On the slides placed in the lower temperature plunge pool, biomats had begun to grow (Fig. 8B), but there was no evidence of silicification or calcite precipitation.

The fast growth rate of the calcite is somewhat curious. If it is assumed that the calcite deposition rate remained constant over the last thirty years, the terrace should be covered with about 30 cm of calcite mineralization. The bottom of the terrace is covered with a much thinner layer of calcite (<2 cm). This indicates that either physicochemical conditions have changed over time, causing slower growth or dissolution of calcite, or initial calcite growth on fresh surfaces is rapid but slows once the layer has been established.

Ngatamariki

The Ngatamariki geothermal system is located 15 km northeast of Wairakei (Fig. 1) and covers an area of about 10 km^2 (Lloyd 1972). Surface emanations at Ngatamariki include hot springs, acid sulfate pools, and warm seeps. The Pavlova spring is the smallest of the hot springs and formed post-1992. Campbell et al. (2002) have described the morphology of the pool, its outflow zone, and associated sinters. The pool is ~ 1.5 m in diameter and 0.5 m in depth. The temperature of the pool in April 2001 was $83 \text{ }^\circ\text{C}$ while the temperature immediately before it enters the Orakonui stream was $50 \text{ }^\circ\text{C}$ (a distance of 10 m). The outflow is shallow (2–10 cm) and lined with chalky-white, meringue-like sinter deposits that extend out over the water surface (Fig. 9A). These deposits are formed of finely laminated silica with lesser amounts of calcite filling interstices between laminations. In cooler areas that remain wet, green, brown, and orange microbial mats are present. Water composition is typical for a dilute chloride–bicarbonate spring with a moderately high chloride and a high HCO_3^- content (Table 2).

Two plastic racks containing glass slides were placed in the spring outflow in April 2001. One rack was located immediately next to the main vent of the spring, where the temperature was $80 \text{ }^\circ\text{C}$. The slides held in this rack remained completely submerged. Samples taken over the ensuing months showed that there was no sinter growth and the slides remained clear. The second rack was positioned about 2 m from the main vent where the water temperature varied from 74 to $77 \text{ }^\circ\text{C}$ over the course of the experiment. In this case, the slides were completely submerged, however, they lay only 2–5 mm below the water surface. By April 2002, the water level had changed substantially (see later in the text) and the tray had tilted so that the remaining slides no longer fully submerged. There was extensive subaerial sinter growth on exposed portion of some slides but it appeared that the tray acted as a barrier to fluid flow and, by July 2002, green bacterial mats had begun to grow.

A modified approach used plastic racks in which glass slides were vertically mounted. These were placed 1 m from

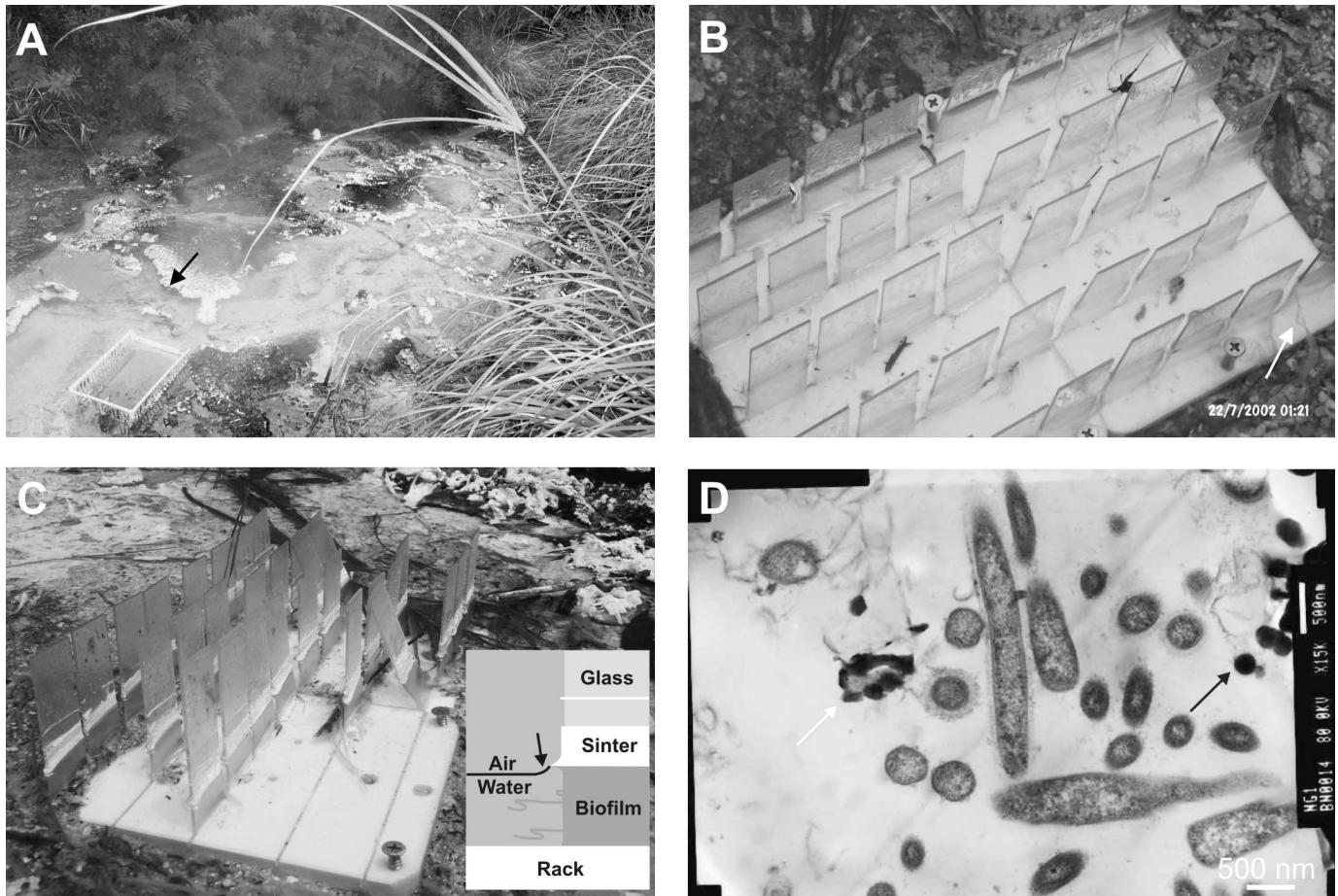
the spring vent in July 2002 and positioned such that half of the slide is exposed to the air while the remainder is submerged (Fig. 9B). The temperature of the water at the bottom of the slides was $71 \text{ }^\circ\text{C}$ while at the top the air temperature was $30 \text{ }^\circ\text{C}$. Six days after placement of the slides, a brownish biofilm had developed on the submerged portion of the slides up to the air–water interface. Also present were long light brown filamentous streamers attached to the slides and moving in the current (Fig. 9Bb). These filaments are unlikely to be cyanobacteria because the water temperature is above their expected maximum tolerance temperature (Winterbourn 1969; Brock and Brock 1971). The portion of the slides above the water surface was completely wetted by condensed steam and water droplets periodically ran down the slides. There was no visible evidence of sinter development on the slides. After 29 days, a thin white line of sinter had formed. This was 7 mm above the air–water interface, indicating that the water level had decreased by this amount between sampling trips. There was no sinter visible at the new air–water interface, and the brown biofilm and streamers were still present on the submerged portion of the slides. In September 2002 (63 days), the water level had dropped 14 mm below the initial level. Above the new air–water interface, a band of silica mineralization 7 mm in width had deposited on the slides, indicating that in the previous month the water level continued to drop but at a slow and constant rate, thereby forming a continuous band of mineralization. On the most recent sampling trip in December 2002 (157 days), the water level had not changed from September. The slides showed growth of a narrow rim of silica sinter (Fig. 9C), which was thickest at the edges of the slides (1.5 mm) and thinner along the faces (0.5 mm). The rims were slightly above the local water level but were in contact with the water by a meniscus that wetted the bottom of the rims (Fig. 9C). Assuming that the time period required for this growth was 94 days, a maximum lateral growth rate of the silica rims of $0.016 \text{ mm day}^{-1}$ is estimated.

TEM examination of rim deposits taken from a slide of September 2002, showed the presence of unmineralized filamentous microbes $0.4 \mu\text{m}$ in diameter with distinct cell walls and extracellular polysaccharide coatings (Fig. 9D). Most of the cells observed in TEM were intact at sampling and unmineralized. Also present are remnants of microbes whose cell walls and sheaths were extensively mineralized by amorphous silica, as well as, numerous silica spherules. The presence of unmineralized intact cells coexisting with mineralized organisms indicates that microbes were living in, or attached to the bottom of, the very small sinter rims.

Tokaanu-Waihi

The Tokaanu-Waihi geothermal system is located near the southern tip of Lake Taupo (Fig. 1) on the northeast margin of the Tongariro volcanic centre. Geothermal features in the area include hot springs, a geyser, areas of steaming ground, fumaroles, and acidic springs (Robinson and Sheppard 1986). In 1942, two shallow test bores (76 and 107 m deep) were drilled north of the hot springs at Tokaanu (Healy 1942). One of the bores is currently active and erupts thermal water continuously to a maximum height of 2 m. At some time after the drilling of the bore, rocks and wood debris were piled up around the wellhead. Silica deposits have built up on this

Fig. 9. Sinters and microbial growth at Ngatamariki. (A) Downstream view of outflow and sinter apron at Pavlova Pool. Orakonui Stream is in the top right corner. Temperature at the slide rack is $\sim 70^\circ\text{C}$. Black arrow points towards meringue-like sinters along the edge of the outflow. Dark areas between sinter are cyanobacterial mats. (B) Racks of glass slides six days after emplacement at 1 m from pool vent ($T = 74^\circ\text{C}$). A thin brown biofilm has grown on the slides below the air–water interface. White arrow points to brown streamers attached to the slides. Glass slides are 25 mm across top dimension. (C) The same two plastic racks shown in (B) after 157 days. Visible silica sinter has grown on the slides and shows that the water level has fluctuated since emplacement. Inset shows a schematic diagram of sinter growths and the position of the meniscus that connects the water to the sinter edge. (D) TEM photomicrograph of microbial growths from the experimental sinter at Ngatamariki. Unmineralized filamentous organisms are surrounded by a mucus coating. Circular cells are due to transverse sectioning through the filaments. Some organisms have been partially replaced by silica spherules (white arrow) and some isolated silica spherules are present (black arrow).



material creating a mound 1.5 m high and 3 m in diameter (Fig. 10A). The central portion of the mound contains a pool of thermal water with a maximum temperature of 100°C through which the geysering water is ejected. The water is chloride rich (Table 2) and represents boiled deep reservoir fluid diluted by shallow groundwater (Severne 1998). The sinter mound provides an excellent example of temperature and hydrodynamic control on microbial populations (Jones et al. 2003). In continuously wetted areas at the center of the mound, the silica is dark brown and is covered with fine spicules ($<2\text{ mm}$). McKenzie et al. (2001) have studied these deposits and described a community of fine filamentous hyperthermophiles living on the silica that is continuously submerged. The dark brown sinter is surrounded by a rim of gray sinter that is breached by the thermal water of the central pool. This flows down the side of the mound in one main, and several smaller, channels, where the silica sinter is white with local patches of dark gray coloration. On the remainder

of the mound, in areas kept continuously wet by splash, the sinter is covered with mottled green to brownish orange microbial mats. Adjacent are dark brown mats in the coolest but continuously wetted areas. It is difficult to collect exact temperature measurements at the transitions between community types because of continuous splash from the vent, but it is clear that temperature is the major control on community distribution (cf. Cady and Farmer 1996). At the bottom of the mound, the thermal water flows out over a sinter apron 40 m long composed of numerous sinter terraces (Fig. 10A). These are defined by 0.5 cm-high sinter rims and are reddish-brown in colour due fine mud washed down from the nearby bank.

In April 2001, a plastic rack containing 18 glass slides was placed on the bottom of the first sinter terrace (Fig. 10A). The slides have remained completely submerged since placement to a depth of 5 mm. Between the bottom of the mound and the sinter rim, the temperature changes from about 80°C ,

Fig. 10. Sinters and microbial growths at Tokaanu. (A) The Healy 2 geyser (G) with surrounding mound composed of silica sinter precipitated on rocks and wood debris. Thermal water flows down the side of the mound and across an extensive sinter apron with numerous terraces (T). Plastic rack containing glass slides was placed on the bottom of the first terrace. Dark band to the left of the rack is a zone of deep green cyanobacteria. (B) Glass slides collected in December 2001 showing growth of thin vitreous silica layer. Darker bands are brownish bacterial growths that grew under the cable ties used to secure the slides (remaining slides are shown in the background). Slide is 75 mm long. (C) Sinter deposit that grew on the low-temperature (40–50 °C) side of the plastic rack (outline of rack impression is shown by the dashed line). Bottom of sinter is composed of silica-cemented coarse sand. This is followed by banded silica. The darker bands are green in colour and suggest the presence of preserved cyanobacteria or their pigments. Alternating dark and light bands are attributed to fluctuations in temperature over time due to changing fluid flux. (D) TEM photomicrograph of transverse cross-section through mineralized filamentous bacteria with thick outer sheaths (S). One of the cells appears mineralized extracellularly but still intact (Ct). The neighbouring cell contains intracellular mineralization. (E) TEM photomicrograph of the larger morphotype of filamentous microbes with isolated silica spherules. These cells are mostly devoid of cytoplasm but their common extracellular sheath and individual cell membranes have survived. (F) TEM photomicrograph of the smaller morphotype of filamentous microbe in transverse section. Most silica mineralization occurs as isolated spherules unattached to bacterial sheaths or membranes.

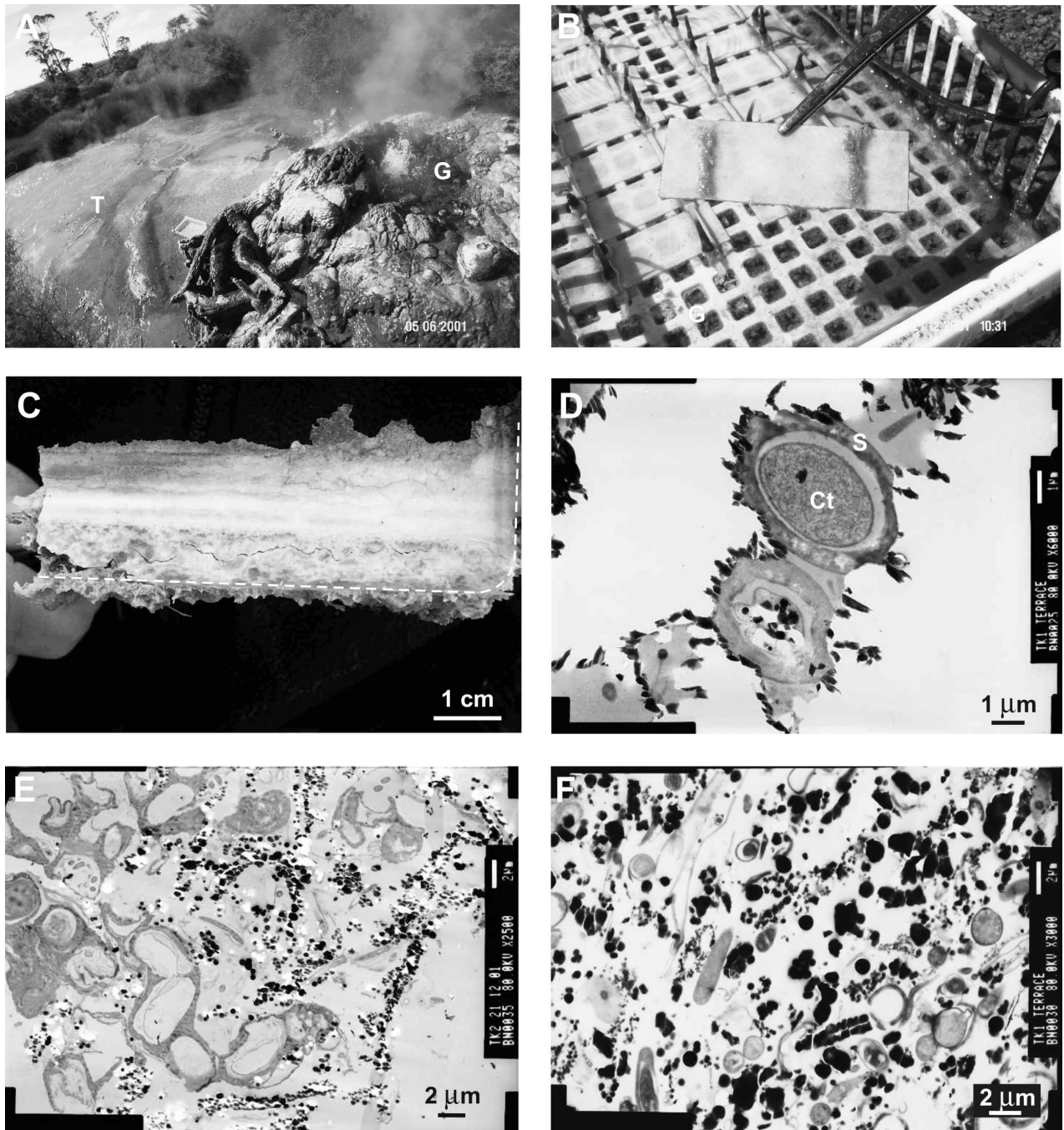
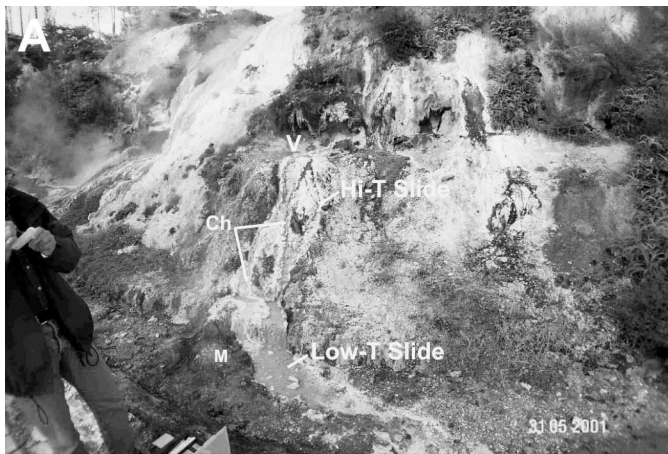


Fig. 11. Sinter growth at Orakei Korako. (A) Photograph showing the Tim and Terry geyser. The vent (V) is covered by an overhang of splash sinter. Thermal water pours continuously down two bifurcated channels (Ch) and into an artificial drain. Adjacent to the channels are green, orange and brown bacterial mats (M). The sinter apron is 1.5 m high. Location of slides in the high-temperature and low-temperature part of the outflow is indicated. (B) Sinter growth on glass slide in the high-temperature ($T \approx 90^\circ\text{C}$) region after 4 months in the Tim and Terry geyser outflow. Most growth appears to have formed by splash. Slide is 25 mm in width.



where thermal water is flowing onto the terrace, to about 50°C . Over this temperature gradient the bottom changes from pink, to brownish orange, to deep green in colour, the latter attributed to thermophilic cyanobacteria bacteria. The rack was placed over the transition from pink sinter to sinter colonized by brown-orange microbial mats. The temperature gradient over the rack in April 2001 was from 60°C nearer the mound to 58°C farthest from the mound. By June 2001, the glass slides had developed a thin vitreous coating of silica.

By December 2001, the vitreous coating of silica had thickened to 0.5 mm (Fig. 10B), and an estimated sinter growth rate of 0.002 mm day^{-1} can be made for this period. The slides also had bands of brownish microbial growths, where the cable ties were located (Fig. 10B). As temperature of the water is unlikely to be significantly different across the length of the slide, this may be due to decreased light flux allowing enhanced growth (Brock 1978). On the subsequent sampling trip, in September 2002, a considerable drop in temperature was noted across the slide rack. At the end closest to the mound, the temperature was now 50°C , and farthest from the mound, the temperature was 44°C . The slides were now covered in visible growths of cyanobacteria. The temperature of the central pool of the geyser had not changed significantly nor had the position of the channels guiding the outflow. The large decrease in temperature is attributed to fluctuations in fluid flux from the geyser. As evidence of this, on the outside of the low-temperature end of the plastic rack a coating of silica sinter had developed (Fig. 10C). The bottom of this deposit is composed of silica-cemented coarse sand that had accumulated next to the rack when placed. This has a mottled green appearance due to the presence of cyanobacteria (Jones et al. 2003). Above this, white and green laminations are present representing organism-poor and organism-rich layers, respectively. These laminations are attributed to variations in fluid flux around the rack causing marked fluctuations in water temperature.

TEM examination of silica deposits from December 2001 showed two microbial morphotypes. The larger was a

filamentous species up to $4\text{ }\mu\text{m}$ in diameter with thick extracellular sheaths ($\sim 0.5\text{ }\mu\text{m}$) and a distinctive cell wall (Fig. 10D). These occurred as isolated cells or as groups of cells within a single extracellular sheath (Fig. 10E). Intact cells containing cytoplasmic material were present, as well as cells in various stages of lysis. In dead cells, the cytoplasm had been lost, but the cell wall remained as a thin membrane detached from the sheath (Figs. 10D, 10E). This detachment is interpreted as an artifact of sample preparation. Silica mineralization was extracellular where it had nucleated on the cellular sheath or it was intracellular in some dead cells (Fig. 10D). In the most heavily silicified areas, silica spherules have coalesced to form opaque fractured rims completely replacing the extracellular sheath. In other areas, the silica mineralization appears to be mostly unrelated to microbial material and fills interstices between dead cells (Fig. 10E). The smaller morphotype is also filamentous but its maximum cell diameter is only about $2\text{ }\mu\text{m}$ (Fig. 10F). These cells have an extracellular sheath up to 200 nm thick. Silicification that occurs where this morphotype is found is mostly extracellular and has not nucleated upon microbial surfaces although some examples of sheath replacement by silica can always be found (Fig. 10F). Although TEM only allows examination of a very small amount of sample material, no areas were found where the two morphotypes coexisted.

Orakei Korako

The Orakei Korako geothermal field is located 25 km northwest of Wairakei (Fig. 1). Active geothermal features include hot pools and springs, several small geysers, mud pools, and steaming ground. Chloride concentrations at Orakei Korako are inherited from a reservoir fluid that is unusually low in chloride for a deep fluid in the TVZ (Hedenquist 1986b). The high HCO_3^- concentration is the result of condensation of CO_2 -rich steam into surface waters, which then mix with the ascending deep fluid before being expelled at the surface.

In April 2001, unrestrained glass slides were placed in the

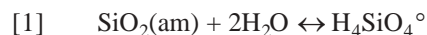
Tim and Terry Geyser outflow (Table 2, Fig. 11A). This geyser is a small vent that continuously ejects a regular flow of thermal water. The vent is covered by a curtain of sinter caused by splash on the overhanging rock. Thermal water flows out over a small ledge and down two small, silica-lined channels ~ 2 m long and 2–10 cm wide. The channels rejoin at the base of the sinter apron and flow a short distance into an artificial drain. Temperature varies along their length between 99 °C at the vent and 76 °C, where the flow enters the drain. The edges of the channels are lined with white to gray nodular sinter that projects out over the water. The sinter is similar to that observed at Ngatamariki in that it overhangs the water surface and is composed of numerous fine laminations. However, it is less friable, of greater thickness, and more irregular in shape than the meringue-like sinters at Ngatamariki. At the bottom of the geyser, adjacent to the sides of the channel, are green and orange bacterial mats, presumably phototrophic bacteria, cyanobacteria, and (or) algae. The temperatures in these areas are consistently < 60 °C. Some overflow from the channel occurs periodically onto the mats and in these areas a white to gray coating of siliceous sinter is present. Beneath this sinter layer, the mats appear to be living.

On our visit in May 2001, lower temperature slides that were completely submerged in the flow near the exit to the artificial channel ($T \approx 76$ °C) were covered in a thin brown coating of calcite. Nearer to the vent, the subaqueous portion of the slides ($T \approx 90$ °C) appeared unaffected while the subaerial portions were covered in vitreous silica. By August 2001, the calcite layer on the lower temperature slides had grown to a thickness of 0.8 mm representing an average growth rate of $0.006 \text{ mm day}^{-1}$ while the subaerial coatings on the higher temperature slides had thickened considerably and consisted of hummocky vitreous amorphous silica. Fig. 11B shows one of these slides in August 2001 (the date stamp on the photo is incorrect), where the average thickness of the sinter had grown to 3 mm. An average sinter growth rate of $0.023 \text{ mm day}^{-1}$ was calculated from this measurement. The subaerially exposed slides at Orakei Korako are the only examples of sinter growth significantly influenced by splash in our experiments.

Discussion

Fluid chemistry, hydrodynamics, and sinter growth rates

The dissolution–precipitation reaction of amorphous silica can be represented by



The equilibrium constant for this reaction is

$$[2] \quad K_{\text{eq}} = a_{\text{H}_4\text{SiO}_4}$$

assuming unit activity for amorphous silica and water. If a dilute solution is in equilibrium with amorphous silica then the concentration of silicic acid is equal to K_{eq} . However, silicic acid may not be the only form of silica in solution. Polymeric silica and silica colloids may also be present. In the Wairakei main drain at Gate 26, 83% of dissolved silica is present as molybdate reactive SiO_2 (E. Mroczek, personal

communication, 2002), assumed to be predominantly $\text{H}_4\text{SiO}_4^\circ$. At the other localities in this study, excluding Champagne Pool, thermal fluids are issuing from pools and bores at temperatures greater than 80 °C. In addition, the time delay before the fluid comes in contact with the slides is short, thus for these localities, essentially all dissolved silica is expected to be monomeric. In Champagne Pool, the residence time of the fluid is unknown, but pH is slightly acid, which inhibits silica polymerization and measurements show that all silica is in its monomeric form (K. Brown, personal communication, 2003).

The equilibrium constants for eq. [2] can be obtained from Gunnarsson and Arnórsson (2000) allowing silicic acid concentration in equilibrium with amorphous silica to be calculated at temperatures between 0 and 300 °C. It can be seen from eq. [2] that amorphous silica solubility is independent of pH. This is true until about pH ≈ 9 at low temperature (<100 °C), where $\text{H}_4\text{SiO}_4^\circ$ begins to deprotonate to form H_3SiO_4^- .

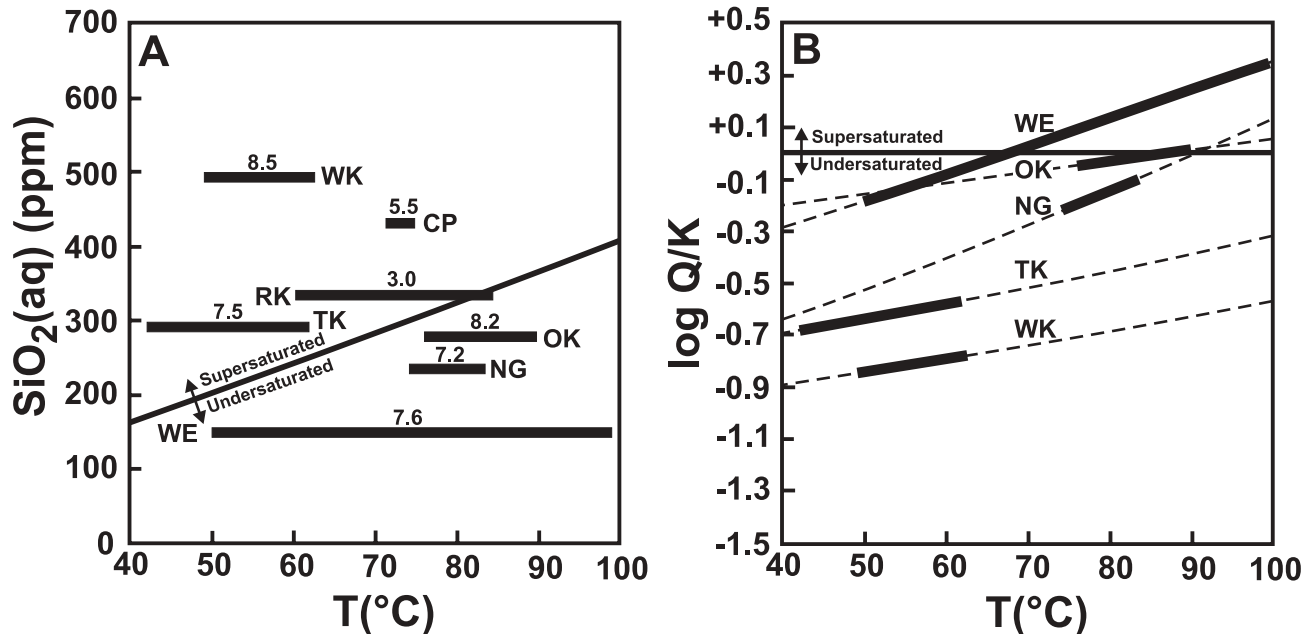
In its simplest form, the rate of silica precipitation can be expressed as

$$[3] \quad \text{Rate}_{\text{ppt}} = -d[\text{H}_4\text{SiO}_4]/dt = -k_{\text{ppt}}[1 - (Q/K_{\text{eq}})]$$

where Q is the ion activity quotient, K_{eq} is the equilibrium constant of reaction (1), and k_{ppt} is the rate constant that is dependent on pH (Iler 1979; Carroll et al. 1998). When $Q/K_{\text{eq}} > 1$, the fluid is supersaturated and amorphous silica will precipitate. If $Q/K_{\text{eq}} = 1$, the fluid has reached equilibrium, and if $Q/K_{\text{eq}} < 1$, the fluid is undersaturated and amorphous silica will dissolve. Thus, the higher the dissolved silica concentration is above saturation, the faster precipitation should occur, all other parameters remaining fixed.

Figure 12A shows the concentration of dissolved monomeric $\text{SiO}_2(\text{aq})$ at each locality plotted versus the range of temperatures encountered. Also shown is the concentration of $\text{SiO}_2(\text{aq})$ in equilibrium with amorphous silica. At Wairakei and Orakei Korako, $\text{SiO}_2(\text{aq})$ is less than the concentration of total silica listed in Table 2 because, at their basic pH values, a significant proportion of silica exists as H_3SiO_4^- . Four localities have $\text{SiO}_2(\text{aq})$ concentrations at or above amorphous silica saturation over their respective temperatures: Wairakei, Tokaanu, Champagne Pool, and Rotokawa. The rate of amorphous silica precipitation at Wairakei is far greater than at any other locality, which is consistent with its high degree of supersaturation ($Q/K_{\text{eq}} = 1.98$ at 62 °C). At Tokaanu ($Q/K_{\text{eq}} = 1.46$ at 55 °C), subaqueous precipitation is occurring but at a much slower rate ($0.002 \text{ mm day}^{-1}$) due to a lower degree of supersaturation. McKenzie et al. (2001) report that there was no silica precipitation on slides placed in the vent pool ($T = 94$ °C in their study) after two weeks. This is consistent with Fig. 12A as at this temperature amorphous silica is undersaturated at Tokaanu. At Champagne Pool, the thermal water is also supersaturated ($Q/K_{\text{eq}} = 1.59$ at 75 °C) and formation of the domal stromatolites beneath the pool surface indicates that subaqueous silicification is occurring (Jones et al. 2001b). To date, there is no evidence of subaqueous silica precipitation on our glass substrates and this suggests that the process is extremely slow at Champagne Pool. This can be explained by the pH dependence of the silica precipitation rate. At acid pH, polymerization and nucleation is inhibited because there is a lesser tendency for the monomeric silicic acid molecule

Fig. 12. Saturation state of thermal waters in this study versus temperature. (A) Concentration of dissolved $\text{SiO}_2(\text{aq})$ at each locality versus the temperature range encountered in each experiment. Solid black line is the equilibrium amorphous silica solubility calculated from Gunnarsson and Arnórsson (2000). Black bars show where amorphous silica is undersaturated (below) and supersaturated (above) with respect to amorphous silica solubility for each locality. Numbers above each bar show the measured pH at each locality. (B) Saturation indices for calcite calculated using the data provided in Table 2. Dashed lines represent saturation index from 40–100 °C based on fluid chemistry. Black bars represent saturation index over the temperature of the experiment. Wk, Wairakei; RK, Rotokawa; CP, Champagne Pool; WE, Waikite; NG, Ngatamariki; TK, Tokaanu; OK, Orakei Korako.



to deprotonate. This also explains the lack of subaqueous sinter formation at Rotokawa. The acid fluids exiting RK2 pool are near saturation with respect to amorphous silica. As they flow over the mud flat, they cool and become supersaturated ($Q/K_{\text{eq}} = 1.23$ at 75 °C), however, the highly acid pH prevents silica precipitation. At the other localities, no subaqueous silica sinter growth was observed on glass substrates, which is consistent with these thermal fluids being undersaturated with respect to amorphous silica at all temperatures encountered. McKenzie et al. (2001) concluded that there is a correlation between the concentration of dissolved silica and the rate at which sinter is deposited. This correlation would be expected according to eq. [3], however, this generalization is only valid if pH is approximately equal between sites.

The preceding discussion refers only to subaqueous sinter growth. Most sinter encountered in the thermal areas in this study is forming subaerially. Other hydrodynamic processes including wave action, capillary action, diffusion, and splash must be invoked to explain their formation. At Champagne Pool, the pool margin is constantly wetted by wave action and during periods of heavy winds, the entire northern sinter rim can be topped by waves. Periodic wetting by thermal water followed by exposure and evaporation can build up a microscopic layer of sinter (Jones et al. 1997). This process affected the experimental substrates placed in Champagne Pool and contributes to the rapid growth rate ($0.023 \text{ mm day}^{-1}$). At Rotokawa and Ngatamariki, wave action is insufficient to supply silica for sinter growth above the water surface. A more plausible explanation is fluid rise due to capillary action, or “wicking” (Hinman and Lindstrom 1996; Campbell et al. 2002). Thermal water is drawn up surfaces and through sinter

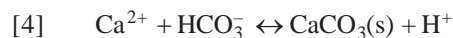
porosity by surface tension. The fluid undergoes evaporation subaerially, dissolved solutes precipitate, and further fluid is drawn upwards. Capillary action would also be expected to contribute to sinter growth at Champagne Pool on more quiescent days. Diffusion can also occur where evaporation is slow relative to diffusion rates of silica through the thermal fluid close to the sinter–water contact, such as at Ngatamariki. On the leading edge of the sinter, where it is in contact with thermal water through a meniscus (Fig. 9C), the water temperature will be lower than the surrounding bulk fluid. If silica is precipitating on the edge, upward diffusion of dissolved silica will occur. This process is similar to the formation of rings when water droplets dry on a surface. Growth rates attributed to capillary and (or) diffusion effects (0.004 and $0.016 \text{ mm day}^{-1}$ for Rotokawa and Ngatamariki, respectively) are slower than by wave action or splash.

Where sinters are formed at geysers or along their turbulent outflows, water splash is the most important mechanism for supplying dissolved silica (Walter 1976; Jones et al. 1997). Hot thermal water begins to cool while still in the air and eventually evaporates on contact with the sinter, forming a microscopic silica deposit. At Orakei Korako, the silica sinter that formed subaerially on the artificial substrates is the result of splash (Fig. 11B) and growth rate is rapid ($0.023 \text{ mm day}^{-1}$).

The processes just mentioned do not require the participation of microorganisms. All of the sinter deposited in our experiments can be explained entirely by equilibrium thermodynamics, reaction kinetics, and the local hydrodynamic regime. Organisms may effect their local environments on the microscopic scale, but there is no evidence that they have

induced precipitation of silica when the bulk chemical conditions predict that it should not occur.

Calcite was also found in two of our experiments (Waikite and Orakei Korako) and is reported as a mineral phase in the meringue sinters at Ngatamariki (Campbell et al. 2002). The precipitation–dissolution reaction of calcite can be represented by



The equilibrium constant for this reaction is

$$[5] \quad K_{\text{Cc}} = \frac{a_{\text{H}^+}}{a_{\text{Ca}^{2+}} \cdot a_{\text{HCO}_3^-}}$$

Unlike silica, the degree of saturation of calcite cannot be represented by one parameter because its solubility is dependent on pH, calcium, and bicarbonate activity. It is necessary to calculate these activities from the composition of the geothermal waters given in Table 2. This was done using the Geochemist's Workbench software package (Bethke 1996). The degree of saturation is represented by the saturation index, $\log Q/K_{\text{Cc}}$.

In Fig. 12B, the saturation index for calcite is plotted against temperature for each locality, excluding Champagne Pool and Rotokawa (acid pH values at these two locations ensure that calcite is highly undersaturated). The most extensive precipitation of calcite was encountered at Waikite artificial terrace. The composition of thermal water issuing from the bore at the eastern end of the terrace shows that the water is $\times 2.5$ supersaturated with respect to calcite. As long as calcite is supersaturated, calcite precipitation is favoured. As the water cools, calcite supersaturation decreases until about 65 °C, below which calcite becomes undersaturated. This assumes that there is no degassing of CO₂ as the water flows across the terrace. If degassing of CO₂ occurs, then pH increases and calcite saturation index similarly increases. Macroscopic observations at Waikite show that at about 60 °C calcite precipitation on the terrace declines and the growth of thick biomats begins. This can be explained by CO₂ degassing maintaining calcite supersaturation to a slightly lower temperature.

At Ngatamariki, calcite occurs as lensoid masses between the laminations of amorphous silica in the meringue sinters. The thermal water in Pavlova pool is undersaturated, albeit slightly, with respect to calcite at its issuance temperature (83 °C, Fig. 12B). As the water flows along the sinter apron and into the Orakonui stream, the temperature drops to 50 °C. Assuming no CO₂ degassing, calcite becomes more undersaturated with decreasing temperature and subaqueous precipitation is not favoured. Campbell et al. (2002) concluded that calcite precipitation must be subaerial between silica laminations due to the “wicking” effect. As a thin film of water migrates up between the silica layers or over the outer surface of the sinter, it must degas CO₂ and becomes saturated with respect to calcite.

Calcite has not been reported as a mineral phase in sinters at Orakei Korako (Lloyd 1972), however, calcite was found on slides retrieved from the lower temperature portion of the Tim and Terry Geyser ($T = 76$ °C). Calcite saturation indices calculated from the fluid composition in Table 2 show that it is supersaturated with respect to calcite at the issuance tem-

perature (99 °C, Fig. 12B). As temperature drops to 76 °C, the fluid passes through calcite saturation and becomes slightly undersaturated. As with Waikite, degassing could cause a rise in pH and maintain calcite saturation to a slightly lower temperature, thus the presence of calcite precipitates is consistent with fluid chemistry.

Also shown in Fig. 12B are the calcite saturation indices for Wairakei and Tokaanu. Calcite is not found in the sinter deposits from either of these localities. This is consistent with the saturation indices at the relevant temperatures.

As with silica, the presence of calcite in the sinter deposits from our experiments can be explained by equilibrium thermodynamics and the hydrodynamic regime. Campbell et al. (2002) and Jones et al. (1996) do not report any microbes in or on calcite from Waikite and Ngatamariki. No evidence has been found of microbes, either cells or mucus, in experimental precipitates from Waikite. It seems reasonable to conclude that calcite mineralization in geothermal sinters from New Zealand is abiotic in origin.

Microbes, minerals, and textural development

Although the precipitation of silica and (or) calcite in New Zealand sinters can be explained by abiotic processes, in areas where opaline silica is precipitating, macroscopic and microscopic evidence show that microbes are present and are undergoing varying degrees of mineralization. The question as to whether this precipitation is passive or metabolically influenced on the microscopic scale cannot be resolved from our results. Nevertheless, it is clear that the presence of microbes greatly influences textural development of the sinters. Other substrates such as rocks, twigs, feathers, rubbish, and plastic racks act as sites for silica precipitation but these eventually become colonized by microorganisms and textural development becomes microbially influenced. For example, at Wairakei, silica precipitation on glass substrates began within a couple of hours of placement. After one day, glass slides became extensively colonized by microbes and eventually all silicification was on microbial surfaces or filled the interstices between mineralized microbes.

The influence of microbial surfaces is variable between sites. The fan-shaped structures at Wairakei are composed entirely of mineralized microbial material and would not have formed without their participation. At Rotokawa, rocks, wood and sinter fragments provide relief above the water surface for the initiation of growth but the development of the microstromatolites is reliant on microorganisms. The textural features of Champagne Pool sinters show a strong dependence on microbes, however, sinter deposits would have formed there in the absence of microbes. Silica and sulfur deposition due to wave action and oxidation of H₂S by atmospheric oxygen are not dependent on biology. At Ngatamariki and Orakei Korako, it is uncertain how strongly microbial influence affects sinter morphology. Processes such as capillary flow, wave action, diffusion, and splash can occur without microbial participation. At Tokaanu, the growth of sinter on the experimental substrates has occurred irrespective of the presence of filamentous bacteria and most of the silica spherules observed by TEM have not nucleated on microbes (Figs. 10E, 10F).

On the microscopic scale, the process of microbial silicification is similar at all locations where observed. Although

the mechanisms of bacteria–silica binding are not yet certain, the initial step is expected to be the bonding of silica monomers to cellular biomolecules. This could be facilitated either by hydrogen bonding between the monomer and functional groups on the cell wall or sheath, or it could be the result of cation bridging through a metal such as calcium or iron (Urrutia and Beveridge 1993; Konhauser and Ferris 1996). In solutions of low ionic strength and neutral to alkaline pH (7–10), these monomers polymerize with further monomeric silica, first as dimers, then cyclic polymers and eventually as small nanospherules (Iler 1979). The nanospherules have varying sizes, with the smaller ones being more soluble and, by the process of Ostwald ripening, a stable spherule size is reached. This is shown best by the silica encasing the bacteria from Wairakei main drain (inset Fig. 2F). The microbes are covered in a continuous layer of amorphous silica composed of numerous coalesced spherules. Later silica spherules deposited on this silica shell are more randomly distributed but of a uniform radius similar to that composing the shell around the microbes. Alternatively, in aged solutions where silica colloids are present, electrostatic bonding to the cell sheath will occur. These will coalesce to form a continuous coating (Phoenix et al. 2000). The remarkably even coatings on the microbes from the Wairakei drain (Fig. 2F) suggest that nucleation was equally distributed over the cell surfaces.

Schultze-Lam et al. (1995) noted that after cell lysis, intracellular mineralization occurs, and they observed that spherules inside the cytoplasm were considerably smaller than those found outside the cell. Nucleation of these spherules would be promoted by the incursion of fluids containing dissolved silica into the high ionic strength environment of the cytoplasm causing rapid “salting-out” of the silica. At Wairakei, both extracellular and intracellular mineralization was observed on larger cyanobacterial cells from the cooler left sub-drain. However, TEM examination of the smaller filaments that make up most of the sinter from the right sub-drain showed that they are composed of solid silica with no observable cytoplasmic space or internal structure. Filament diameter increases from 100 nm when they are unmineralized (Fig. 2E) to about 500 nm within two days (Fig. 2F). If it is assumed that these were microorganisms, the absence of any internal structure could be due to the lack of a resistant cellular sheath or wall and complete replacement of the cell wall and cytoplasmic space by silica. If all extracellular porosity were filled by further amorphous silica then there would be no evidence of the existence of these organisms and the sinter would appear microbe-free. Samples from Tokaanu also showed extracellular and intracellular mineralization associated with the larger sheathed cyanobacteria (Fig. 10D).

At Champagne Pool, experimental growths on glass substrates mimic those found along the pool margin. Filamentous microbes that attach and grow on all available surfaces dominate the subaqueous portion. These become coated with a layer of orange sulfur, the origin of which is uncertain (Mountain et al. 2001). It is possible that it is the result of a metabolic process, such as the oxidation of H_2S to colloidal sulfur. Colloidal sulfur has a high surface area and can react with dissolved metals in the water. If metals, such as As, Sb, Au, Ag, Tl, and Hg, are being carried in the pool water as

hydrosulfide complexes (cf. Seward 1982; Krupp and Seward 1990), then polymerization of the sulfide ligand to colloidal sulfur leads to metal incorporation. This suggests that the high concentrations of heavy metals encountered in the orange sediments may be indirectly linked to microbial metabolism.

Native sulfur accumulates on the pool margin at the air–water interface. A similar band of yellow sulfur was found on the slides and is composed of euhedral crystals that fine upwards (Figs. 7A, 7E). This sulfur is quite different from the orange precipitates in that it is bright yellow in colour (it lacks high concentrations of heavy metals); euhedral in form, and much larger than any associated microbes (implying that it is abiotic in origin); and has grown in situ. The upward decrease in crystal size can be explained by a similar decrease in residence time in the pool water due to wave action. Native sulfur along the pool margin is found on the portion of the rim washed by wave action. Its growth is attributed to inorganic oxidation of H_2S from the pool water due to exposure to atmospheric oxygen in the wash zone. The lack of metal enrichment and hence the yellow color can be explained by lower surface areas, intermittent exposure to pool water, and the low reactivity of this crystalline sulfur.

Microbes and their associated mucus and cannulae covered the surface of the native sulfur crystals (Figs. 7E, 7D). As the sulfur crystals increase in size and number, these microbes would become incorporated into the sulfur layer and sulfurized remnants may be present. The location of these microbes is probably not fortuitous and suggests that there could be a metabolic relationship between the sulfur and the microbes.

A sharp change from sulfur to silica mineralization implies a significant change in physicochemical conditions. The average rate at which silica accumulates subaerially is rapid ($0.023 \text{ mm day}^{-1}$). Wave action is the only plausible explanation for this rapid accumulation. The sharp boundary represents the mean pool level, about which a constantly shifting temperature gradient oscillates, the amplitude dependent on wave height. Silica precipitation occurs where exposure, evaporation, cooling, and precipitation outpaces periodic submersion in the thermal water. Once even the smallest amount of silica precipitates by evaporation and cooling, it will not re-dissolve on submersion because the water is supersaturated. Nucleation would be rapid and spherule size would be quite small explaining the lack of visible spherules (under SEM examination) on the slides. Sulfide oxidation occurs below this level where thermal water is exposed to atmospheric oxygen. On calm days, the contribution of wave oscillations would be limited, with most silica being supplied by capillary rise and evaporation. This would result in slow sinter growth, mineralization of microbes in the porous layers, and colonization by microorganisms on the wetted outer surfaces of spicules. As wave amplitude increases, the portion of the slide being mineralized would increase, eventually forming a complete carapace over the entire exposed surface. Cady and Farmer (1996) noted that the highest concentration of microbial remains is found at the tips of spicules. This is reflected on our slides, where the layers of laminated silica along the sides are microbe-poor (Fig. 7F), and the tops of the slides showed abundant microbes (Fig. 7H). The maximum tolerance temperature of the microbes inhabiting the subaerial portion of the slides is expected to be lower than the pool temperature.

It is not known whether these microbes can tolerate periodic immersion in the water but those growing on the tips would be submerged less often, allowing them to grow more extensively. On a very windy day, constant wash would deposit droplets of thermal water on the sides and tips of the spicules. These would not easily penetrate the microbial mesh due to the surface tension of the fluid. Evaporation and cooling would build up a layer of silica essentially devoid of microbes and create underlying pore space. This process is reflected in the microbe-rich and microbe-poor layers found in natural spicules (Cady and Farmer 1996; Jones et al. 1997; Mountain et al. 2001) and in our experimental analogs (Fig. 7G).

The microstromatolites at Rotokawa also display spicule growth although the average rate is estimated to be very slow ($0.004 \text{ mm day}^{-1}$). They differ from microstromatolites from Champagne Pool in that they are quite hard and do not have any visible porosity (Figs. 5C, 5D). Jones et al. (2000) estimated a growth rate of spicules from the south side of the hot spring lake of $0.0003 \text{ mm day}^{-1}$ based on pollen grains entrapped in the sinter. This is not necessarily incongruous with our estimate as the latter is based on lateral growth perpendicular to the slide and not vertical growth of individual spicules. The growth of visible spicules did not occur on our slides until after a few months and, thus, the slower rate estimated here may be comparable. Nevertheless, it is clear that sinter growth rate at Rotokawa is extremely slow. The lack of wave action requires that capillary rise followed by evaporation must be responsible for sinter growth. As the water evaporates and cools, silica nanospherules inevitably nucleate due to increasing supersaturation, however, at low pH these do not grow past 2–3 nm in diameter (Iler 1979). Microbes, clay minerals, and sulfur would be coated and in-filled with small nanospherules, resulting in exceptional preservation of microbial and mineral fabrics (Jones et al. 2000). This would also explain the hard, non-porous nature of the microstromatolites.

Experimental slides at Ngatamariki showed rapid development of a continuous biofilm below the water surface with no evidence of silicification. This biofilm grew right up to the air–water interface, including the meniscus that forms between the sinter and the surrounding water level (Fig. 9C). Silica deposition on filamentous microbes at the air–water interface due to cooling, evaporation, or possibly diffusion of dissolved silica into the cooler meniscus would build a small rim around objects in the pool. Campbell et al. (2002) described silicified, subhorizontal filaments $\sim 1 \mu\text{m}$ in diameter in the porous layers from spicules at Ngatamariki. This is consistent with TEM observation of 500 nm, unsilicified, filamentous microbes in the biofilm and sinter growths from our experimental slides (Fig. 9D). These layers would form when microbial growth outpaces silicification and may be related to periods when slight fluctuations in water level cause the meniscus to detach from the rim. Once it is reestablished, the condensed steam layer and the hot pool water would become continuous and silica could diffuse into the microbial layer. This would facilitate silicification of the subaerial microbial layer on the top of the sinter rim. Nodular sinter from the Tim and Terry geyser at Orakei Korako displays textures identical to those found at Ngatamariki. This indicates that capillary rise is possible in areas where waters are more turbulent and splash is occurring. The growth of thin abiotic

layers of silica is related to abundant splash but the growth of interlayer spicules and in-filling with silica is caused by capillary rise.

Although most of the experimental mineralization at Tokaanu is subaqueous, the development subaerially of cyanobacteria-rich sinter deposits on the bars and sides of the plastic rack is of interest (Fig. 10C). Wetting of the rack side due to capillary rise and steam condensation creates an environment for cyanobacterial growth above the surrounding water surface. This film of bacteria would “creep” up the side of the rack forming an upwardly thinning layer. Similarly, diffusion of silica up through the bacterial layer would cause slow mineralization of the filament sheaths and inter-filament porosity. The maintenance of a thin wet biofilm by a continuous thin coating of water along vertical surfaces means that cyanobacterial films can survive and be silicified above the surrounding average water level.

The experimental results show that mesoscopic and microscopic textural development of silica sinters is strongly influenced by the presence of thermophilic organisms. These act primarily as sites of surface nucleation and hence, the larger the bacterial surface area, the more rapid the growth of sinter. However, this must be qualified by considering inorganic controls such as the degree of supersaturation, temperature, and pH on silica precipitation rates. The rate of growth, development of microscopic textures, and the degree of bacterial preservation are, thus, an interplay between the microbial community present and inorganic controls. In waters that are supersaturated with respect to amorphous silica, low temperature, and (or) low pH results in silica nucleation as abundant small nuclei that do not undergo Ostwald ripening and form a dense silica matrix that accurately preserves microbial material (cf. Phoenix et al. 2000; Jones et al. 2000). At intermediate to high temperature and neutral to alkaline pH, rapid nucleation of silica nuclei occurs, but these undergo Ostwald ripening, increasing in size and decreasing in number. This results in progressive destruction of microbial remnants and poorer preservation (e.g., Fig. 10D).

Conclusions

New Zealand hot springs display a wide variety of sinter deposit morphologies. The origin of these different morphologies and the rates at which they have grown have been investigated by a combination of field measurements and experimental studies. The experimental studies have been undertaken in situ at seven geothermal areas, including Wairakei Power Station main wastewater drain, Champagne Pool at Waiotapu, Rotokawa, Waikite, Ngatamariki, Tokaanu, and Orakei Korako. In these areas, a range of water chemistries, temperatures, and hydrodynamic regimes is present and allows comparison of sinter growth rates and textural development from a variety of environments. Except at Waikite, silica sinter developed on glass slides from all localities. At Wairakei and Tokaanu, all sinter growth on glass slides was subaqueous. At Champagne Pool, there was no significant subaqueous sinter development but subaerial growth was present. At all other localities (except Waikite), silica sinter grew subaerially. At Waikite and Orakei Korako, calcite was found as a precipitate on submerged slides without silica. Sulfur occurs at Champagne Pool both as orange coatings on filamentous anaerobic

microorganisms and as a rim at the air–water interface of the pool. Heavy metal enrichment is attributed to interaction between colloidal sulfur produced by microbial metabolism and dissolved heavy metals in the pool.

Sinter growth rates from all areas are summarized as follows: Wairakei (10 mm day⁻¹ or 350 kg a⁻¹ m⁻² of drain wall); Champagne Pool (0.023 mm day⁻¹ subaerial); Rotokawa (0.004 mm day⁻¹ subaerial); Waikite (0.026 mm day⁻¹ subaqueous calcite); Ngatamariki (0.016 mm day⁻¹ subaerial); Tokaanu (0.002 mm day⁻¹ subaqueous); Orakei Korako (0.023 mm day⁻¹ subaerial, 0.006 mm day⁻¹ subaqueous calcite).

The precipitation of subaqueous silica sinter or calcite mineralization can be successfully predicted by equilibrium thermodynamic principles. This implies that, although microorganisms may be present, they have not induced subaqueous precipitation where predicted not to occur. In general, the rate of silica precipitation can be correlated with the degree of supersaturation with respect to amorphous silica, however, the inhibitory or enhancing effects of pH must be considered before comparing rates from different localities. The fastest rates of sinter growth occurred in areas where hydrodynamic effects were dominant. Wave action at Champagne Pool and splash at Orakei Korako are the principle causes of sinter development at these localities. In other areas where subaerial growth has occurred, capillary rise and diffusion are invoked as the dominant hydrodynamic mechanisms for sinter growth. Once a surface is wetted and undergoes cooling and evaporation, rapid nucleation of silica occurs on all available surfaces, including microorganisms. These nanospherules of silica do not undergo Ostwald ripening and form fine grained coatings with a high propensity to preserve microbial fabrics. In contrast, in subaqueous sinter formation, spherules grow in size and decrease in number due to Ostwald ripening. This creates a relatively uniform size distribution of larger silica spherules and leads to the destruction of microbial remnants such that smaller organisms are not likely to be preserved.

Acknowledgments

This study would not have been possible without the assistance of Duncan Graham and Edward Mroczek of IGNS, New Zealand. Field sampling and laboratory assistance for phylogenetic work was provided by Emma Summers of HortResearch, New Zealand. Maqsudul Alam and Stuart Donachie of the University of Hawaii provided guidance and assistance for phylogenetic work. Imaging was done with the assistance of Eric Condliffe, School of Earth Sciences, and Adrian Hick, School of Biology, at the University of Leeds. Analytical work was performed by Moya Appleby, Marshall Muller, and Ann Noddings of the IGNS Water/Gas Analytical Laboratory, Wairakei, New Zealand. We thank Lew Bacon and Contact Energy Ltd. (Wairakei), Tauhara Trust B (Rotokawa), Jim Climo (Ngatamariki), Richard Fulton (Waiotapu), Mark Bowie (Waikite), Bob Hayes (Tokaanu), and Craig Gibson (Orakei Korako) for access. Sampling permission was granted by the Department of Conservation, Tongariro and Bay of Plenty Conservancies, New Zealand. Sarah Gleeson and Vernon Phoenix provided valuable reviews of the manuscript. BWM acknowledges funding from the Foundation for Research in Science and Technology (Contract C05X0201: Geothermal for the New Millennium) and from

the NSOF Extremophiles Programme. LGB acknowledges financial support from the United Kingdom Natural Environment Research Council Grant No. GR9/04623.

References

- Altschul, S.F., Gish, W., Miller, W., Myers, E.W., and Lipman, D.J. 1990. Basic local alignment search tool. *Journal of Molecular Biology*, **215**: 403–410.
- Benning, L.G., Phoenix, V., Yee, N., Tobin, M.J., Konhauser, K.O., and Mountain, B.W. 2002. Molecular characterization of cyanobacterial cells during silicification: a synchrotron-based infrared study. *In Proceedings of the geochemistry of the Earth's surface conference*, Honolulu, Hawaii, May 20–24, 2002, pp. 259–263.
- Bethke, C.M. 1996. *Geochemical Reaction Modelling: Concepts and Applications*. Oxford University Press, Oxford, U.K.
- Brock, T.D. 1978. *Thermophilic Microorganisms and Life at High Temperatures*. Springer-Verlag, New York.
- Brock, T.D., and Brock, M.L. 1971. Microbiological studies of thermal habitats of the central volcanic region, North Island, New Zealand. *New Zealand Journal of Marine and Freshwater Research*, **5**: 233–258.
- Broda, D.M., Lawson, P.A., Bell, R.G., and Musgrave, D.R. 1999. *Clostridium frigidicarnis* sp. nov., a psychrotolerant bacterium associated with “blown pack” spoilage of vacuum-packed meats. *International Journal of Systematic Bacteriology*, **49**: 1539–1550.
- Cady, S.L., and Farmer, J.D. 1996. Fossilization processes in siliceous thermal springs: trends in preservation along thermal gradients. *In Evolution of hydrothermal ecosystems on Earth (and Mars?)*. Edited by G.R. Brock and J.A. Goode. John Wiley, Chichester, U.K., pp. 150–173.
- Campbell, K.A., Rodgers, K.A., Brotheridge, J.M.A., and Browne, P.R.L. 2002. An unusual modern silica–carbonate sinter from Pavlova spring, Ngatamariki, New Zealand. *Sedimentology*, **49**: 835–854.
- Carroll, S., Mroczek, E., Alai, M., and Ebert, M. 1998. Amorphous silica precipitation (60 to 120 °C): Comparison of laboratory and field rates. *Geochimica et Cosmochimica Acta*, **62**: 1379–1396.
- Ferris, F.G., Beveridge, T.J., and Fyfe, W.S. 1986. Iron-silica crystallite nucleation by bacteria in a geothermal sediment. *Nature (London)*, **320**: 609–611.
- Giggenbach, W., and Goguel, R.L. 1989. 4th Ed. *Collection and Analysis of Geothermal and Volcanic Waters and Gas Discharges*. Report No. CD2401, Chemistry Division, Department of Scientific and Industrial Research, Petone, New Zealand.
- Glover, R.B., Klyen, L.E., and Crump, M.E. 1992. The location and geochemistry of natural features in the Waikite geothermal system. Department of Scientific and Industrial Research, Chemistry Technical Report No. 92/14 (unpublished).
- Gunnarsson, I., and Arnórsson, S. 2000. Amorphous silica solubility and the thermodynamic properties of H₄SiO₄° in the range of 0° to 350 °C at P_{sat}. *Geochimica et Cosmochimica Acta*, **64**: 2295–2307.
- Healy, J. 1942. Boron in hot springs at Tokaanu, Lake Taupo, New Zealand. *New Zealand Journal of Science and Technology*, **B2**: 1–17.
- Hedenquist, J.W. 1986a. Waiotapu geothermal field. *In Guide to the active epithermal (geothermal) systems and precious metal deposits of New Zealand*. Edited by R.W. Henley, J.W. Hedenquist, and P.J. Roberts. Monograph Series on Mineral Deposits, **26**, pp. 65–79.
- Hedenquist, J.W. 1986b. Orakeikorako geothermal field. *In Guide to the active epithermal (geothermal) systems and precious metal deposits of New Zealand*. Edited by R.W. Henley, J.W. Hedenquist,

- and P.J. Roberts. Monograph Series on Mineral Deposits, 26, pp. 113–120.
- Hedenquist, J.W., and Henley, R.W. 1985. Hydrothermal eruptions in the Waiotapu geothermal system, New Zealand: Their origin, associated breccias and relation to precious metal mineralization. *Economic Geology*, **80**: 1640–1668.
- Hinman, N.W., and Lindstrom, R.F. 1996. Seasonal changes in silica deposition in hot springs. *Chemical Geology*, **132**: 237–246.
- Iler, R.K. 1979. *The Chemistry of Silica, Solubility, Polymerization, Colloid and Surface Properties, and Biochemistry*. John Wiley, New York.
- Inagaki, F., Hayashi, S., Doi, K., Motomura, Y., Eiji, I., and Ogata, S. 1997. Microbial participation in the formation of siliceous deposits from geothermal water and analysis of the extremely thermophilic bacterial community. *FEMS Microbiology Ecology*, **24**: 41–48.
- Jones, B., Renaut, R.W., and Rosen, M.R. 1996. High-temperature (>90 °C) calcite precipitation at Waikite Hot Springs, North Island, New Zealand. *Journal of the Geological Society of London*, **153**: 481–496.
- Jones, B., Renaut, R.W., and Rosen, M.R. 1997. Biogenicity of silica precipitation around geysers and hot spring vents, North Island, New Zealand. *Journal of Sedimentary Research*, **67**: 88–104.
- Jones, B., Renaut, R.W., and Rosen, M.R. 1998. Microbial biofacies in hot-spring sinters: A model based on Ohaaki Pool, North Island, New Zealand. *Journal of Sedimentary Research*, **68**: 413–434.
- Jones, B., Renaut, R.W., and Rosen, M.R. 1999a. Actively growing siliceous oncoids in the Waiotapu geothermal area, North Island, New Zealand. *Journal of the Geological Society of London*, **156**: 89–103.
- Jones, B., Renaut, R.W., and Rosen, M.R. 1999b. Role of fungi in the formation of siliceous coated grains, Waiotapu geothermal area, North Island, New Zealand. *Palaios*, **14**: 475–492.
- Jones, B., Renaut, R.W., and Rosen, M.R. 2000. Stromatolites forming in acidic hot-spring waters, North Island, New Zealand. *Palaios*, **15**: 450–475.
- Jones, B., Renaut, R.W., and Rosen, M.R. 2001a. Microbial construction of siliceous stalactites at geysers and hot springs: Examples from Whakarewarewa geothermal area, North Island, New Zealand. *Palaios*, **16**: 73–94.
- Jones, B., Renaut, R.W., and Rosen, M.R. 2001b. Biogenicity of gold- and silver-bearing siliceous sinters forming in hot (75 °C) anaerobic spring-waters of Champagne Pool, Waiotapu, North Island, New Zealand. *Journal of the Geological Society (of London)*, **158**: 895–911.
- Jones, B., Renaut, R.W., and Rosen, M.R. 2003. Silicified microbes in a geyser mound: The enigma of low-temperature cyanobacteria in a high-temperature setting. *Palaios*, **18**: 87–109.
- Konhauser, K.O., and Ferris, F.G. 1996. Diversity of iron and silica precipitation by microbial mats in hydrothermal waters, Iceland: Implications for Precambrian iron formations. *Geology*, **24**: 323–326.
- Konhauser, K.O., Phoenix, V.R., Bottrell, S.H., Adams, D.G., and Head, I.M. 2001. Microbial–silica interactions in Icelandic hot spring sinter: possible analogues for some Precambrian siliceous stromatolites. *Sedimentology*, **48**: 415–433.
- Krupp, R., and Seward, T.M. 1987. The Rotokawa geothermal system, New Zealand: An active epithermal gold-depositing environment. *Economic Geology*, **82**: 1109–1129.
- Krupp, R., and Seward, T.M. 1990. Transport and deposition of metals in the Rotokawa geothermal system, New Zealand. *Mineralium Deposita*, **25**: 73–81.
- Lane, D.J. 1991. 16S/23S rRNA sequencing. *In* *Nucleic acid techniques in bacterial systematics*. Edited by E. Stackebrandt and M. Goodfellow. John Wiley and Sons, New York, pp. 115–175.
- Lloyd, E.F. 1972. Geology and hot springs of Orakeikorako. *New Zealand Geological Bulletin*, **85**: 1–164.
- McKenzie, E.J., Brown, K.L., Cady, S.L., and Campbell, K.A. 2001. Trace metal chemistry and silicification of microorganisms in geothermal sinter, Taupo Volcanic Zone, New Zealand. *Geothermics*, **30**: 483–502.
- Mountain, B.W., Benning, L.G., and Graham, D.J. 2001. Biomineralization in New Zealand geothermal areas. *In* *Proceedings 23rd New Zealand Geothermal Workshop*, Auckland, New Zealand, pp. 27–32.
- Pancost, R.D., Pressley, S., Coleman, J.M., Benning, L.G., and Mountain, B.W. 2002. Bacterial and archaeal adaptations to extreme conditions at New Zealand hot springs. *Proceedings of the 2002 William Smith Meeting: Life in Earth: Energy, Minerals, Mars and the Deep Biosphere*. Geological Society (of London).
- Phoenix, V.R., Konhauser, K.O., and Adams, D.G. 1999. Photosynthetic controls on the silicification of cyanobacteria. *In* *Geochemistry of the Earth's surface*. Edited by H. Armannsson. A.A. Balkema, Rotterdam, The Netherlands, pp. 275–278.
- Phoenix, V.R., Adams, D.G., and Konhauser, K.O. 2000. Cyanobacterial viability during hydrothermal biomineralization. *Chemical Geology*, **169**: 329–338.
- Prescott, L.M., Harley, J.P., and Klein, D.A. 2002. *Microbiology*. McGraw-Hill, New York.
- Robinson, B.W., and Sheppard, D.S. 1986. A chemical and isotopic study of the Tokaanu-Waihi geothermal area, New Zealand. *Journal of Volcanology and Geothermal Research*, **27**: 135–151.
- Renaut, R.W., Jones, B., and Rosen, M.R. 1996. Primary silica oncoids from Orakeikorako hot springs, North Island, New Zealand. *Palaios*, **11**: 446–458.
- Schultze-Lam, S., Ferris, F.G., Konhauser, K.O., and Wiese, R.G. 1995. In situ silicification of an Icelandic hot spring microbial mat: implications for microfossil formation. *Canadian Journal of Earth Sciences*, **32**: 2021–2026.
- Severne, C.M. 1998. Recent geochemical investigations of the Tokaanu-Waihi geothermal field. *In* *Proceedings of the 20th New Zealand Geothermal Workshop*, Auckland, New Zealand, pp. 251–258.
- Seward, T.M. 1982. The transport and deposition of gold in hydrothermal ore solutions. *In* *Gold '82*. Edited by R.P. Forster. A.A. Balkema, Amsterdam, The Netherlands, pp. 165–181.
- Smith, B.Y., Rodgers, K.A., and Browne, P.R.L. 2001. Opal-A — The first 100 days. *In* *Proceedings of the 23rd New Zealand Geothermal Workshop*, Auckland, New Zealand, pp. 131–136.
- Stetter, K.O. 1998. Hyperthermophiles: Isolation, classification and properties. *In* *Extremophiles: microbial life in extreme environments*. Edited by K. Horikoshi and W.D. Grant. John Wiley & Sons, New York, pp. 1–24.
- Urrutia, M.M., and Beveridge, T.J. 1993. Mechanism of silicate binding to the bacterial cell wall in *Bacillus Subtilis*. *Journal of Bacteriology*, **175**: 1936–1945.
- Walter, M.R. 1976. Geysers of Yellowstone National Park: An example of abiogenic stromatolites. *In* *Stromatolites*. Edited by M.R. Walter, *Developments in Sedimentology*, **20**: 87–112.
- Walter, M.R., Bauld, J., and Brock, T.D. 1972. Siliceous algal and bacterial stromatolites in hot spring and geyser effluents of Yellowstone National Park. *Science (Washington, D.C.)*, **179**: 402–405.
- Weed, W.H. 1889. Formation of travertine and siliceous sinter by the vegetation of hot springs. *United States Geological Survey, 9th Annual Report*, pp. 613–676.

- Weissberg, B.G. 1969. Gold-silver ore-grade precipitates from New Zealand thermal waters. *Economic Geology*, **64**: 95–108.
- Wilson, C.J.N, Houghton, B.F., McWilliams, M.D., Lanphere, S.D., Weavers, S.D., and Briggs, R.M. 1995. Volcanic and structural evolution of the Taupo Volcanic Zone, New Zealand: a review. *Journal of Volcanology and Geothermal Research*, **68**: 1–28.
- Winterbourn, M.J. 1969. The distribution of algae and insects in hot spring thermal gradients at Waimangu, New Zealand. *New Zealand Journal of Marine and Freshwater Research*, **3**: 459–465.
- Yee, N., Phoenix, V.R., Konhauser, K.O., Benning, L.G., and Ferris, F.G. 2003. The effect of cyanobacteria on silica precipitation at neutral pH: Implications for bacterial silicification in geothermal hot springs. *Chemical Geology*. In press.